`UNI`: Unlearning-based Neural Interpretations

Ching Lam Choi[*]
CSAIL, Department of EECS
Massachusetts Institute of Technology
chinglam@mit.edu

Alexandre Duplessis
Department of Computer Science
University of Oxford
alexandre.duplessis@cs.ox.ac.uk

Serge Belongie
Pioneer Centre for AI
University of Copenhagen
s.belongie@di.ku.dk

Abstract

Gradient-based interpretations often require an anchor point of comparison to avoid saturation in computing feature importance. We show that current baselines defined using static functions—constant mapping, averaging or blurring—inject harmful colour, texture or frequency assumptions that deviate from model behaviour. This leads to accumulation of irregular gradients, resulting in attribution maps that are biased, fragile and manipulable. Departing from the static approach, we propose `UNI` to compute an (un)learnable, debiased and adaptive baseline by perturbing the input towards an *unlearning direction* of steepest ascent. Our method discovers reliable baselines and succeeds in erasing salient features, which in turn locally smooths the high-curvature decision boundaries. Our analyses point to unlearning as a promising avenue for generating faithful, efficient and robust interpretations.

1 Introduction

The utility of large models is hampered by their lack of explainability and robustness guarantees. Yet breakthroughs in language modelling (Meta, 2024; Anthropic, 2024; Jiang et al., 2023; Google, 2024; Achiam et al., 2023) and generative computer vision (Rombach et al., 2022; Liu et al., 2023; Deepmind, 2024; Brooks et al., 2024) yield promising high-stakes applications, spanning domains of healthcare, scientific discovery, law and finance. As such, being able to interpret these models has become a primary concern for researchers, policymakers and the general populace, with international calls for explainability, accountability and fairness in AI decision-making (European Commission, 2021; White House OSTP, 2022; Bengio et al., 2023). To this end, recent works focus on the 2 main directions of making models *inherently explainable* (Böhle et al., 2022; Brendel & Bethge, 2018; Koh et al., 2020; Bohle et al., 2021; Chen et al., 2019; Ross et al., 2017) and *post-hoc interpretable* (Bau et al., 2017; Kim et al., 2018; Zhou et al., 2018; Ghorbani et al., 2019b). Unfortunately, the former is marred by the status quo of proprietary models and prohibitive training costs. This motivates seeking robust attributions which reliably explain model predictions, to facilitate better risk assessment and trade-off calibration (Böhle et al., 2022; Doshi-Velez & Kim, 2017).

Post-hoc methods explain a black-box model's output by attributing its decision back to predictive features of the input. They achieve this via leveraging components of the model itself (*e.g.* gradients and activations), or through approximation with a simpler, interpretable simulator. A desirable post-hoc explanation should exhibit *high faithfulness* – to be rationale-consistent (Yeh et al., 2019; Atanasova et al., 2020) with respect to a model's decision function; *low sensitivity* – to yield reliably similar saliency predictions for input features in the same local neighbourhood (Alvarez Melis & Jaakkola, 2018; Ghorbani et al., 2019b); *low complexity* – the explanation should be functionally simpler and more understandable than the original black-box model (Bhatt et al., 2021).

Gradient-based saliency methods are widely used for feature attribution, due to their simplicity, efficiency and post-hoc accessibility. This can be further decomposed into 3 families: perturbative, backpropagative and path-based, which we detail in Section 6. Gradient-based attribution is intuitive since the first-order derivative reveals which features significantly influence the model's classification decision. However, naively using local gradients yields unfaithful attributions due to saturation, where the non-linear output function flattens in vicinity of the input and zero gradients are

---

[*]Research work completed during an internship at the Pioneer Centre for AI and University of Copenhagen.
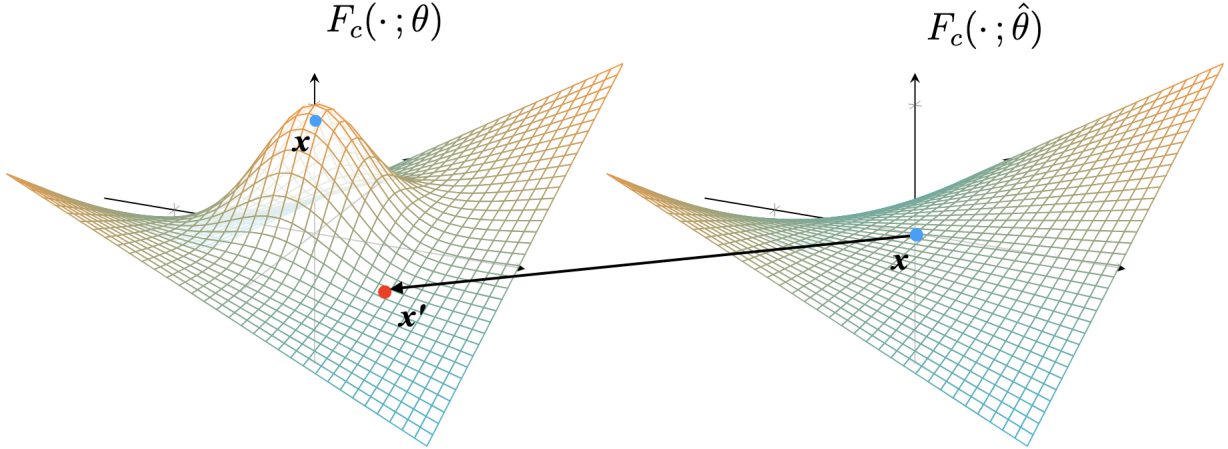
$$F_c(\cdot\,;\theta) \qquad\qquad F_c(\cdot\,;\hat{\theta})$$

Figure 1: *Left:* Confidence of original model θ at image x and baseline x'. *Right:* Confidence of *unlearned* model $\hat{\theta}$ at image x. After unlearning in the model space $\theta \longmapsto \hat{\theta}$, we optimise the baseline to match the unlearned input confidence, such that $F_c(x';\theta) \approx F_c(x;\hat{\theta})$.

computed (Sundararajan et al., 2017; 2016). To improve gradient-sensitivity, later methods introduce a baseline input for reference, and backpropagate the difference in activation scores on a path between the reference and image-of-interest (Shrikumar et al., 2016; Sundararajan et al., 2017). The baseline is chosen to be devoid of predictive features and far away from the saturated local neighbourhood. However, such methods accumulate gradient noise when interpolating from the baseline to the input, leading to high local sensitivity (Ancona et al., 2018). Consequently, attribution maps become disconnected, sparse and irregular, where the saliency scores fluctuate wildly between neighbouring pixels of the same object and are visually noisy (Adebayo et al., 2018). This noise accumulation has two root causes—a *poorly chosen baseline* and *high-curvature output manifold* along the path features. Previous works (Sturmfels et al., 2020; Xu et al., 2020) have sought better baselines by empirically comparing between using a black image, a gaussian noised image, a gaussian blurred image, a uniformly noised image, an inverted colour image, as well as averaging attributions over several baseline choices. However, the correct baseline to represent a lack of salient features depends heavily on the specific classification task, on the trained model and on the input image. Indeed, the optimal baseline varies for each task–model–image combination (Akhtar & Jalwana, 2023); the baseline problem remains largely unsolved. Turning to the second problem of high-curvature output manifold, because trained neural networks exhibit approximately piece-wise linear decision boundaries (Goodfellow et al., 2014), therefore inputs near function transitions are vulnerable to perturbative attacks. By simply adding norm-bounded, imperceptible adversarial noise to the input image, attackers can dramatically alter the attribution map without changing the model's class prediction (Ghorbani et al., 2019a; Dombrowski et al., 2019). Methods of mitigation include explicit smoothing via averaging over multiple noised gradient attributions (Smilkov et al., 2017); adaptively optimising the integration path of attribution (Kapishnikov et al., 2021); imposing an attribution prior during training and optimising it at each step (Erion et al., 2021). However, all of these proposals starkly increase the complexity of attribution, requiring computationally costly forward and backward propagation steps.

To tackle the problematic triad of *1. post-hoc attribution biases, 2. poor baseline definition, 3. high-curvature output manifold*, we propose UNI to discover debiased baselines by locally *unlearning* inputs, *i.e.* perturbing them in the unlearning direction of steepest ascent, as visualised in Figure 1. Towards better baselines, our unlearned reference is by definition explicitly optimised to lower output class confidence and can empirically erase or occlude salient features. We also say that the unlearned baseline is specific and featureless w.r.t. each task–model–input combination. Unlike the practice of using a black image baseline—which creates a post-hoc colour bias that darker pixels are less likely to be salient, UNI does not impose additional, pixel-wise colour, scale or geometric assumptions that are not already present in the model itself. Finally, we address the high-curvature decision boundaries problem by realising that this is a product of the training process—targeted unlearning smooths the decision boundary of the model within the vicinity of the input. For a more detailed overview on the principle of machine unlearning, we refer the reader to Section 6 of the supplement. We empirically verify this local smoothing effect by measuring the normal curvature of the model function before and after unlearning; we also demonstrate that unlearning makes attributions resistant to perturbative attacks. Our contributions can be summarised as follows:

1. *Post-hoc attribution can impose new biases.* We approach the baseline challenge from the fresh lens of post-hoc biases. We show that static baselines (*e.g.* black, blurred, random noise) inject additional colour, texture and frequency assumptions that are not present in the original model's decision rule, which leads explanation infidelity and inconsistency.

2. *A well-chosen baseline is specific and featureless.* We establish theoretically grounded principles for sound baseline definitions, by formalising the idea of an "absence of signal" through an unlearning direction of steepest ascent in model loss. By unlearning predictive features in the model space and matching this reference model's activations with a perturbation in the input space, we introduce a new definition of "feature absence" and a novel attribution algorithm.

3. *Unlearning reduces the curvature of decision boundaries and increases robustness.* Targeted unlearning simulates the function statistics of unseen data, and smooths the curvature of the output manifold around the sample. This is characterised by low geodesic curvature of the path and bounded principal curvature of the output surface. This points to reduced variability of the gradient vector under small-norm input perturbations, leading to better attribution robustness and faithfulness.

2 Preliminaries

We consider feature attribution for trained deep neural networks within image classification. Informally, we seek to assign scores to each pixel of an image for quantifying the pixel's influence (sign and magnitude) on the predicted output class confidence. It is noteworthy that attributions can be signed: a negative value indicates that removing the pixel increases the target class probability.

2.1 Notation

The input (feature) space is denoted as $\mathcal{X} \subset \mathbb{R}^{d_X}$, where d_X is the number of pixels in an image. The output (label) space is $\mathcal{Y} \subset \mathbb{R}^{d_Y}$; $\mathcal{Y}$ is the set of all probability distributions on the set of classes. The model space is denoted as $\mathcal{F} \subset \mathcal{Y}^{\mathcal{X}}$. A trained model $F : x \mapsto (F_1(x), ..., F_{d_Y}(x))$ returns the probability score $F_c(x)$ of each class c. Attribution methods are thus functions $\mathcal{A} : \{1, ..., d_X\} \times \mathcal{F} \times \{1, ..., d_Y\} \times \mathcal{X} \to \mathbb{R}$, where $\mathcal{A}(i, F, c, x)$ is the importance score of pixel i of image x for the prediction made by F_c. For convenience, we use the shorthand $\mathcal{A}_i(x)$ to refer to the attributed saliency score of a pixel i for a specific class prediction $c \in \{1, ..., d_Y\}$. We express a linear path feature as $\gamma(x', x, \alpha) : \mathbb{R}^{d_X} \times \mathbb{R}^{d_X} \times [0, 1] \to \mathbb{R}^{d_X}$, where $\gamma = (1 - \alpha)x' + \alpha x$ and employ shorthands $\gamma(0) = x', \gamma(1) = x$.

3 Gradient-based Attributions in a Nutshell

3.1 Limitations

Taking the local gradients of a model's output confidence map $F_c(x)$ – for target class c – is a tried and tested method for generating explanations. Commonly termed Simple Gradients (Erhan et al., 2009; Baehrens et al., 2010; Simonyan et al., 2013), $\mathcal{A}_i^{\text{SG}}(x) = \nabla_{x_i} F_c(x)$ can be efficiently computed for most model architectures. However, it encounters output saturation when activation functions like ReLU and Sigmoid are used, leading to zero gradients (hence null attribution) even for important features (Sundararajan et al., 2017; 2016). DeepLIFT (Shrikumar et al., 2016) reduces saturation by introducing a "reference state". A feature's saliency score is decomposed into positive and negative contributions by backpropagating and comparing each neuron's activations to that of the baseline. Integrated Gradients (IG) (Sundararajan et al., 2017) similarly utilises a reference, black image and computes the integral of gradients interpolated on a straight line between the image and the baseline.

$$\mathcal{A}_i^{\text{IG}}(x) = (x_i - x_i') \int_{\alpha=0}^{1} \nabla_{x_i} F_c \left(x' + \alpha(x - x') \right) \, d\alpha \tag{1}$$

Practically, the integral is approximated by a Riemann sum. Of existing methods, IG promises desirable, game-theoretic properties of "sensitivity", "implementation invariance", "completeness" and "linearity". We consequently focus
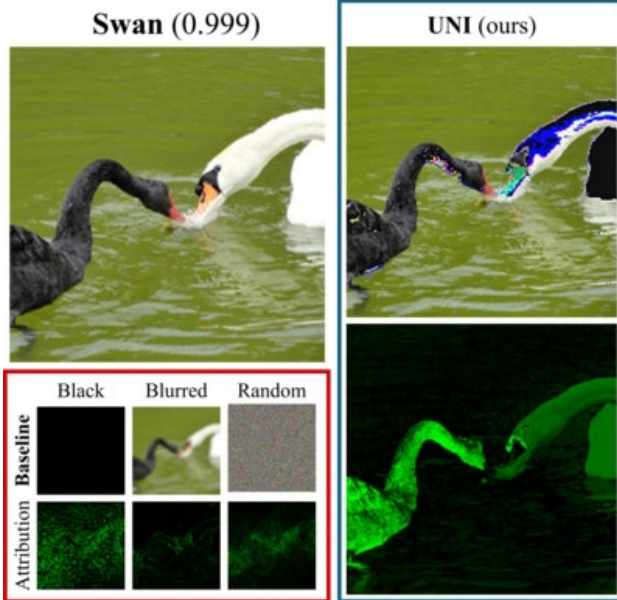
Figure 2: We visualise post-hoc biases imposed by static baselines—black baseline (colour), blurred (texture), random (frequency). `UNI` learns to mask out predictive features used by the model, generating reliable attributions.

Algorithm 1 `UNI`: unlearning direction, baseline matching and path-attribution

1: **Given** model $F(\cdot, \theta)$; inputs (x, y)

2: **Choose** unlearning step-size η;
PGD steps T, budget ϵ, step-size μ;
Riemann approximation steps B

3: **Initialise** perturbation δ^0

4: **Unlearning direction.** $\hat{\theta} = \theta + \eta \frac{\nabla_\theta \mathcal{L}(F_c(x;\theta), y)}{\|\nabla_\theta \mathcal{L}(F_c(x;\theta), y)\|}$

5: **for** $t = 0, \cdots, T-1$ **do**

$$\mathcal{C} = D_{KL}(F(x; \hat{\theta}) \parallel F(x + \delta^t; \theta))$$
$$\delta^{t+1} = \delta^t - \mu \nabla_\delta \mathcal{C}$$
$$\delta^{t+1} = \varepsilon \frac{\delta^{t+1}}{\|\delta^{t+1}\|}$$

6: **end for**

7: **Baseline** definition $x' = x + \delta^T$

8: **Attributions** computation:

$$\mathcal{A}_i^{\text{UNI}}(x) = \frac{(x_i - x_i')}{B} \sum_{k=1}^{B} \nabla_{x_i} F_c\left(x' + \frac{k}{B}(x - x'); \theta\right)$$

on analysing and developing the IG framework, though the proposal to unlearn baselines can be applied to most mainstream gradient-based saliency methods. Despite the advantages of IG, its soundness depends on a good *baseline definition*—an input which represents the "absence" of predictive features; also on having stable *path features*—a straight-line of increasing output confidence along the path integral from baseline to target image. In the conventional setting where a black image is used, Akhtar & Jalwana (2023) prove that IG assumptions are violated due to ambiguous path features, where extrema of model confidences lie along the integration path instead of at the endpoints of the baseline (supposed minimum) and input image (supposed maximum). Sturmfels et al. (2020) enumerate problems with other baselines obtained via gaussian blurring, maximum distance projection, uniform noise. Despite the diversity of baseline alternatives, no candidate is optimal for each and every attributions setting. For instance, models trained with image augmentations (*e.g.* colour jittering, rescaling, gaussian blur) yield equivalent or even higher confidences for blurred and lightly-noised baselines—we need baselines that are well-optimised for each task–model–input combination. Without principled baselines, problems of non-conformant intermediate paths and counter-intuitive attribution scores will doubtlessly persist.

3.2 Post-hoc Biases are Imposed

Since the baseline represents an absence of or reduction in salient features, static baseline functions (*e.g.* black, blurred, noised) implicitly assume that similar features (*e.g.* dark, smooth, high-frequency) are irrelevant for model prediction. To illustrate this intuition, we can consider IG with a black baseline, wherein it becomes more difficult to attribute dark but salient pixels. Due to the colour bias that "near-black features are unimportant", the term $(x_i - x_i')$ is small and requires a disproportionately large gradient $\nabla_{x_i} F_c(\cdot)$ to yield non-negligible attribution scores. Indeed, this is what we observe in Figures 2, 3, 8, where darker features belonging to the object-of-interest cannot be reliably identified. We further empirically verify that each static baseline imposes its own post-hoc bias by experimenting on ImageNet-C (Hendrycks & Dietterich, 2019). Corresponding to the 3 popular baseline choices for IG (all-black, gaussian blurred, gaussian noised), we focus on the families of *digital* (brightening and saturation), *blur* (gaussian and defocus blur) and *noise* (gaussian and shot noise) common-corruptions. Figures 4, 9 demonstrate that IG with a blurred baseline fails to attribute blurred inputs due to saturation and overly smoothed image textures; Figures 5, 10 visualise how a noised IG baseline encounters high-frequency noise and outputs irregular, high-variance attribution scores, even for adjacent

pixels belonging to the same object. We crucially emphasise that such colour, texture and frequency biases are not present naturally in the pre-trained model but rather injected implicitly by a suboptimal choice of static baseline. The observation that poor baseline choices create *attribution bias* has so far been overlooked. As such, we depart entirely from the line of work on alternative static baseline towards adaptively (un)learning baselines with gradient-based optimisation. *UNI eliminates all external assumptions except for the model's own predictive bias.*
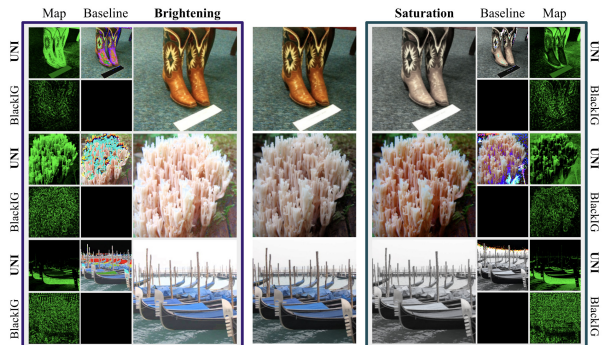
Figure 3: When the brightness or saturation is altered, IG with a black baseline fails to identify dark features, such as the boat's hull (R3) or the top of the boot (R1).

Table 1: **Path monotonicity scores** with Spearman correlation coefficient (higher = better). Integrating from a "featureless" baseline to the sample should give a path of monotonically increasing prediction confidence.

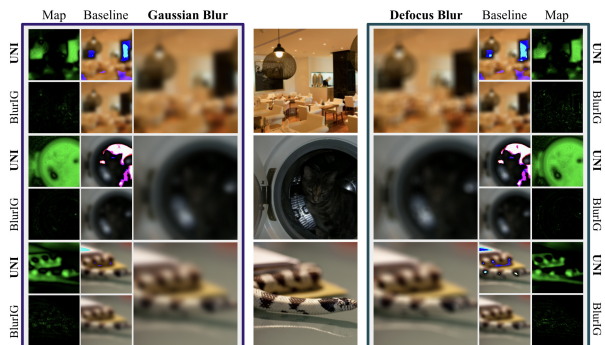|	UNI	IG	BlurIG	GIG
ResNet-18	**.97** $\pm$.222	.69 $\pm$.460	.57 $\pm$.576	.45 $\pm$.476
Eff-v2-s	**.95** $\pm$.258	.28 $\pm$.615	.34 $\pm$.613	.38 $\pm$.437
ConvNeXt-T	**.99** $\pm$.121	.76 $\pm$.379	.77 $\pm$.486	.46 $\pm$.485
VGG-16-bn	**.94** $\pm$.286	.69 $\pm$.474	.60 $\pm$.544	.46 $\pm$.479
ViT-B-16	**.89** $\pm$.396	.71 $\pm$.399	.27 $\pm$.648	.44 $\pm$.468
SwinT	**.97** $\pm$.189	.88 $\pm$.326	.88 $\pm$.482	.45 $\pm$.474

Figure 4: Under gaussian or defocus blur, IG with a blurred baseline suffers from saturation; has overly smooth texture; does not yield meaningful features.
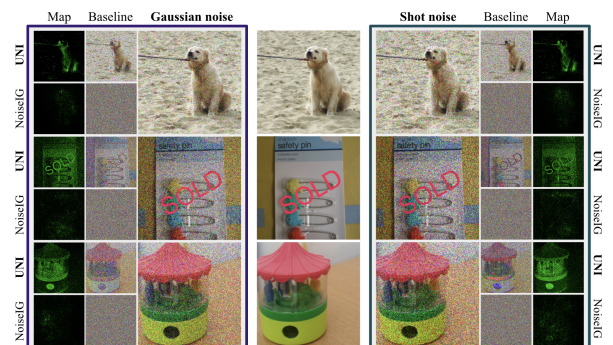

Figure 5: Gaussian and shot noise create visual artifacts prominent in noised-baseline IG. Frequency bias leads to disparate scores for adjacent pixels.

4 UNI: Unlearning-based Neural Interpretations

4.1 Baseline desiderata

A desirable baseline should preserve the game-theoretic properties of path-attribution (Section 3.1) and refrain from imposing post-hoc attribution biases (Section 3.2). For every given task-model-image triad, a well-chosen baseline should be *1. image-specific*—be connected via a path feature of low curvature to the original image; *2. reflect only the model's predictive biases*—salient image features should be excluded from the baseline; be *3. less task-informative than the original image*—interpolating from the baseline towards the input image should yield a path of increasing predictive confidence. We now introduce the UNI pipeline: first, unlearn predictive information in the model space; then, use activation-matching between unlearned and trained models to mine a featurelesss baseline in the image space; finally, interpolate along the low-curvature, conformant and consistent path from baseline to image to compute reliable explanations in the attributions space.

4.2 Desirable Path Features

Proximity   The meaningfulness of the attributions highly depends on the meaningfulness of the path. We aim for a smooth transition between absence and presence of features; and this intuitively cannot be achieved if the baseline and input are too far apart. (Srinivas & Fleuret, 2019) formalizes this intuition through the concept of *weak dependence*, and proves that this property can only be compatible with completeness in the case where the baseline and the input lie in the same connected component (in the case of piecewise-linear models). An obvious implementation of this proximity condition in the general case is to bound the distance $||x - x'||$ to a certain value ε. This is strictly enforced in Algorithm 1 by normalizing the perturbation at each step t.

Low Curvature.   The curvature of the model prediction along the integrated path has been identified (Dombrowski et al., 2019) as one of the key factors influencing both the sensitivity and faithfulness of the computed attributions. We substantiate the intuition that a smooth and regular path is preferred by analysing the Riemannian sum calculation. Assuming that the function $g : \alpha \in [0,1] \mapsto \nabla F_c(x' + \alpha(x - x'))$ is derivable with a continuous derivative (i.e. $\mathcal{C}^1$) on the segment $[x', x]$, elementary calculations and the application of the Taylor-Lagrange inequality give the following error in the Riemann approximation of the attribution,

$$\left| (x_i - x_i') \int_{\alpha=0}^{1} g(\alpha)\, d\alpha - \frac{(x_i - x_i')}{B} \sum_{k=1}^{B} g\left(\frac{k}{B}\right) \right| \leq \frac{M||x - x'||^2}{2B} \tag{2}$$

where $M = \max_{\alpha \in [0,1]} \frac{\mathrm{d}g}{\mathrm{d}\alpha} = \max_{\alpha \in [0,1]} \frac{\partial^2 F_c(x' + \alpha(x - x'))}{\partial \alpha^2}$ exists by continuity of g' on $[0,1]$.

Thus, lower curvature along the path implies a lower value of the constant M, which in turn implies a lower error in the integration calculation. A smaller value B of Riemann steps is needed to achieve the same precision. More generally, a low curvature (i.e. eigenvalues of the hessian) on and in a neighborhood of the baseline and path reduces the variability of the calculated gradients under small-norm perturbations, increasing the sensitivity and consistency of the method. Empirically, we observe a much lower curvature of the paths computed by UNI, as can be seen in Table 1 and Appendix Figures 17, 18, 19, 20, 21, 22. Figure 7 also confirms the increased robustness to Riemann sum error induced.

Monotonic.   Intuitively, the path γ defined by interpolating from the "featureless" baseline x' to the input image x should be *monotonically increasing* in output class confidence; the cumulative attribution score should similarly increase. At the image level, for all j, k such that $j \leq k$, since $|\gamma(j) - x| \geq |\gamma(k) - x|$, therefore the predictive confidence should be non-decreasing and order-preserving: $F_c(\gamma(j)) \leq F_c(\gamma(k))$. Constraining γ to be monotonically increasing suffices to satisfy criteria for *valid path features* (Akhtar & Jalwana, 2023). Zooming in on input feature $\tilde{x}_i = \gamma(\tilde{k})_i$ on the linear path for $\tilde{k} < 1$, since the gradient of γ is always positive and x_i maximises F_c on the interval, therefore both conditions $\mathrm{sgn}(\nabla_{x_i} F_c(x_i)) \cdot \mathrm{sgn}(\nabla_{\tilde{x}_i} F_c(\tilde{x}_i)) = 1$ and $|\nabla_{x_i} F_c(x_i)| > |\nabla_{\tilde{x}_i} F_c(\tilde{x}_i)|$ are naturally met. This is crucial for preserving the *completeness axiom* of Integrated Gradients (Sundararajan et al., 2017), that attribution scores add up to the difference quantity $\sum_{i=1}^{d_x} \mathcal{A}_i(x) = F_c(x) - F_c(x')$, and that attribution score $\mathcal{A}_i(x)$ is only non-zero when x_i contributes to the prediction. Completeness does not hold when path features are non-conformant, *i.e.* $F_c(\gamma(j)) > F_c(\gamma(k))$; or when extremities exist along γ, *i.e.* for $\tilde{k} \in (0,1)$, $F_c(\gamma(\tilde{k})) > F_c(\gamma(1))$ or $F_c(\gamma(\tilde{k})) < F_c(\gamma(0))$.

5   Experiments

We experiment on ImageNet-1K (Deng et al., 2009), ImageNet-C (Hendrycks & Dietterich, 2019) and compare against various path-based and gradient-based attribution methods. This includes IG (Sundararajan et al., 2017), BlurIG (Xu et al., 2020), GIG (Kapishnikov et al., 2021), AGI (Pan et al., 2021), GBP (Springenberg et al., 2014) and DeepLIFT (Shrikumar et al., 2016). We consider a diverse set of pre-trained computer vision backbone models (Paszke et al., 2019), including ResNet-18 (He et al., 2016), EfficientNet-v2-small (Tan & Le, 2021), ConvNeXt-Tiny (Liu et al., 2022), VGG-16-bn (Simonyan & Zisserman, 2015), ViT-B_16 (Dosovitskiy et al., 2020) and Swin-Transformer-Tiny (Liu et al., 2021). Unless otherwise specified, we the following hyperparameters: unlearning step size $\eta = 1$; l_2 PGD with $T = 10$ steps, a budget of $\varepsilon = 0.25$, step size $\mu = 0.1$; Riemann approximation with $B = 15$ steps. Our results verify UNI's high faithfulness, stability and robustness.

5.1 Faithfulness

We report MuFidelity scores ([Bhatt et al., 2021](#)), *i.e.* the faithfulness of an attribution function $\mathcal{A}$, to a model F, at a sample x, for a subset of features of size $|S|$, given by $\mu_f(F, \mathcal{A}; x) = \text{corr}_{S \in \binom{[d]}{|S|}} \left(\sum_{i \in S} \mathcal{A}(i, F, c, x), \ F_c(x) - F_c(x_{[x_s = \bar{x}_s]}) \right)$. We record the (absolute) correlation coefficient between a randomly sampled subset of pixels and their attribution scores. As from Table 2, UNI outperforms other methods across all settings but one, indicating high faithfulness. We supplement these numbers with visual comparisons in Appendix Figures [11](#), [12](#), [13](#), [14](#), [15](#), [16](#) against IG (black and noised baselines), BlurIG, GIG, AGI, GBP, DeepLift.

Table 2: *MuFidelity scores* measure the correlation between a subset of pixels' impact on the output (*i.e.* change in predictive confidence) and assigned saliency scores. Since attribution methods can yield strong positive or negative correlation, we report the absolute scores.

	UNI	IG	BlurIG	GIG	AGI	GBP	DeepLIFT
ResNet-18	**.12** ±.124	.06 ±.068	.07 ±.076	.07 ±.080	.10 ±.110	.09 ±.094	.08 ±.082
EfficientNetv2s	**.06** ±.046	.05 ±.043	.05 ±.044	.05 ±.044	.06 ±.045	.05 ±.043	.05 ±.043
ConvNeXt-Tiny	.16 ±.115	.11 ±.086	.15 ±.121	**.18** ±.149	.17 ±.131	.09 ±.072	.11 ±.084
VGG-16-bn	**.18** ±.141	.08 ±.066	.09 ±.076	.13 ±.108	.14 ±.104	.13 ±.108	.10 ±.082
ViT-B_16	**.15** ±.114	.10 ±.074	.10 ±.077	.11 ±.079	.14 ±.104	.09 ±.070	.10 ±.072
Swin-T-Tiny	**.13** ±.100	.09 ±.071	.12 ±.102	.12 ±.104	.13 ±.102	.09 ±.069	.10 ±.076

5.2 Robustness

Next, we evaluate UNI's robustness to fragility adversarial attacks on model interpretations. Following [Ghorbani et al. (2019a)](#), we design norm-bounded attacks to maximise the disagreement in attributions whilst constraining that the prediction label remains unchanged. We consider a standard l_∞ attack designed with FGSM ([Goodfellow et al., 2014](#)), with perturbation budget $\epsilon_f = 8/255$.

$$\delta_f^* = \arg \max_{\|\delta_f\|_p \leq \epsilon_f} \frac{1}{d_X} \sum_{i=1}^{d_X} d\left(\mathcal{A}(i, F, c, x), \mathcal{A}(i, F, c, x + \delta_f) \right) \tag{3}$$

$$\text{subject to} \quad \arg \max_{c'} F_{c'}(x) = \arg \max_{c} F_{c'}(x + \delta_f) = c$$

We report robustness results using 2 distance measures—Spearman correlation coefficient in Figure [3](#) and top-k pixel intersection score in Figure [4](#)—pre and post attack. While other methods like DeepLIFT (DL), BlurIG, Integrated Gradients (IG) are misled to output irrelevant feature saliencies, UNI robustly maintains attribution consistency and achieves the lowest attack attribution disagreement scores (before and after FGSM attacks) for both metrics.

Table 3: *Robustness*: Spearman's correlation coefficient. Higher scores indicate better path consistency pre/post FGSM attacks.

	UNI	IG	BlurIG	SG	DeepL
ResNet-18	**.271**	.088	.084	.014	.139
Eff-v2-s	**.302**	.009	.076	.008	.018
ConvNeXt-T	**.292**	.010	.127	.011	.012
VGG-16-bn	**.290**	.143	.098	.014	.108
ViT-B-16	**.319**	.018	.066	.023	.023
SwinT	**.271**	.088	.084	.014	.139

Table 4: *Robustness*: Top-1000 pixel intersection. Higher percentages indicate better attribution reliability pre/post FGSM attacks.

	UNI	IG	BlurIG	SG	DeepL
ResNet-18	**37.3**	20.0	25.3	18.2	24.8
Eff-v2-s	**39.4**	17.4	23.3	18.6	18.0
ConvNeXt-T	**34.8**	15.0	26.2	16.7	15.1
VGG-16-bn	**35.7**	25.5	25.3	18.8	25.2
ViT-B-16	**40.7**	17.1	21.7	19.6	17.2
SwinT	**37.3**	20.0	25.3	18.2	24.8

5.3 Stability

We compare UNI and other methods' sensitivity to Riemann approximation noise, which manifests in visual artifacts and misattribution of salient features. As seen from Figures [6](#), [7](#), UNI reliably finds unlearned, "featureless" baselines for
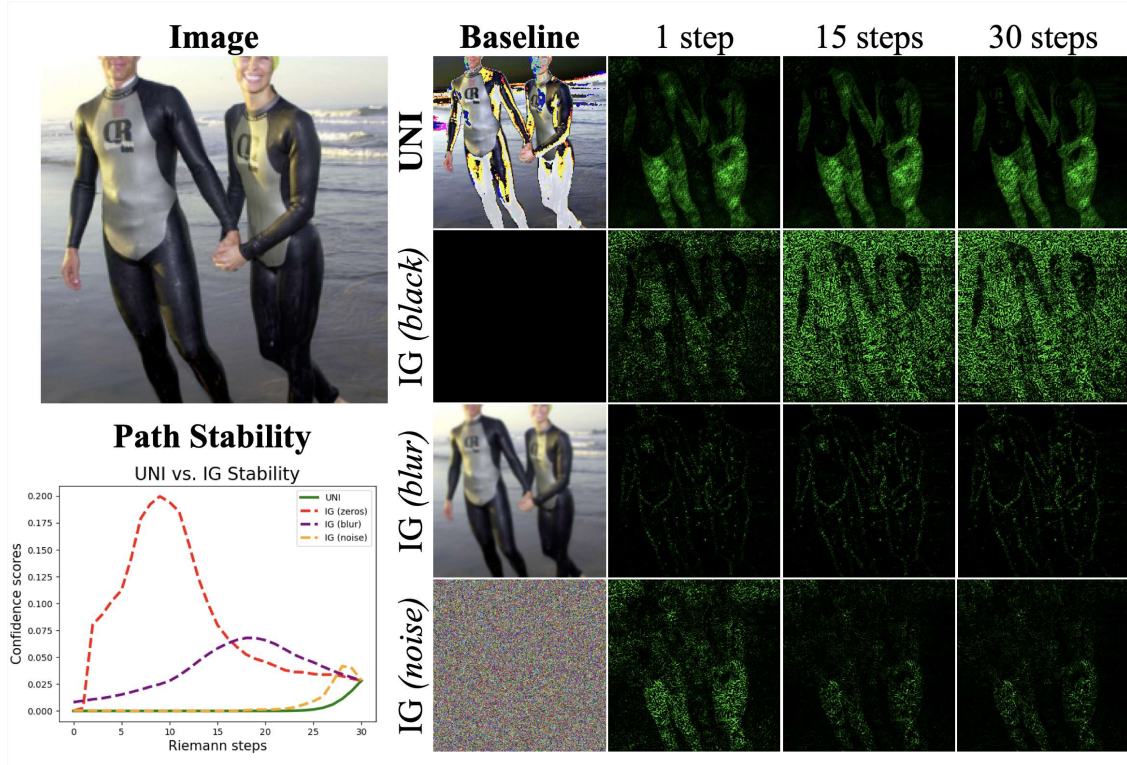
Figure 6: `UNI` path features monotonically increase in output confidence when interpolating from baseline to input. This eliminates instability and inconsistency problems caused by extrema and turning points along the Riemann approximation path, which is present in other methods.

consistent attribution, regardless of the number of approximation steps $B \in \{1, 15, 30\}$. This is due to the low geodesic curvature of $\gamma^{\texttt{UNI}}$, which approximately minimises the local distance between points used in Riemann approximation.

6 Related Work

Machine unlearning. We draw inspiration from the high-level principle of unlearning, which concerns the targeted "forgetting" of a data-point for a trained model, by localising relevant information stored in network weights and introducing updates or perturbations (Bourtoule et al., 2021). Formally, machine unlearning can be divided into exact and approximate unlearning (Nguyen et al., 2022). Exact unlearning seeks indistinguishability guarantees for output and weight distributions, between a model not trained on a sample and one that has unlearned said sample (Ginart et al., 2019; Thudi et al., 2022; Brophy & Lowd, 2021). However, provable exact unlearning is only achieved under full re-training, which can be computationally infeasible. Hence, approximate unlearning was proposed stemming from ϵ-differential privacy (Dwork, 2011) and certified removal mechanisms (Guo et al., 2020; Golatkar et al., 2020). The former guarantees unlearning for $\epsilon = 0$, *i.e.* the sample has null influence on the decision function; the latter unlearns with first/second order gradient updates, achieving max-divergence bounds for single unlearning samples. Unlearning naturally lends itself to path-based attribution, to localise then delete information in the weight space, for the purposes of defining an "unlearned" activation. This "unlearned" activation can be used to match the corresponding, "featureless" input, where salient features have been deleted during the unlearning process. While the connection to interpretability is new, a few recent works intriguingly connect machine unlearning to the task of debiasing classification models during training and evaluation (Chen et al., 2024; Kim et al., 2019; Bevan & Atapour-Abarghouei, 2022).

Perturbative methods. Perturbative methods perturb inputs to change and explain outputs (Sculley et al., 2015), including LIME (Ribeiro et al., 2016), SHAP, KernelSHAP and GradientSHAP (Lundberg et al.), RKHS-SHAP (Chau et al., 2022), ConceptSHAP (Yeh et al., 2020), InterSHAP (Janzing et al., 2020), and DiCE (Kommiya Mothilal et al., 2021). LIME variants optimise a simulator of minimal functional complexity able to match the black-box model's local behaviour for a given input-label pair. SHAP (Lundberg et al.) consolidates LIME, DeepLIFT (Shrikumar et al., 2016), Layerwise Relevance Propagation (LRP) (Montavon et al., 2019) under the general, game-theoretic framework of additive feature attribution methods. For this framework, they outline the desired properties of local accuracy, missingness, consistency; they propose SHAP values as a feature importance measure which satisfies these properties under mild assumptions to generate model-agnostic explanations. However, such methods fail to give a global insight of the model's decision function and are highly unstable due to the reliance on local perturbations (Fel et al., 2022). Bordt et al. (2022) show that this leads to variability, inconsistency and unreliability in generated explanations, where different methods give incongruent explanations which cannot be acted on.

Backpropagative methods. Beginning with simple gradients (Erhan et al., 2009; Simonyan et al., 2013), this family of methods—also, LRP (Montavon et al., 2019), DeepLIFT (Shrikumar et al., 2016), DeConvNet (Zeiler & Fergus, 2014), Guided Backpropagation (Springenberg et al., 2014) and GradCAM (Selvaraju et al., 2017)—leverages gradients of the output $w.r.t.$ the input to proportionally project predictions back to the input space, for some given neuron activity of interest. Gradients of neural networks are, however, highly noisy and locally sensitive – they can only crudely localise salient feature regions. While this issue is partially remedied by SmoothGrad (Smilkov et al., 2017), we still observe that gradient-based saliency methods have higher sample complexity for generalisation than normal supervised training (Choi & Farnia, 2024) and often yield inconsistent attributions for unseen images at test time.

Path-based attribution. This family of post-hoc attributions is attractive due to its grounding in cooperative game-theory (Friedman, 2004). It comprises Integrated Gradients (Sundararajan et al., 2017), Adversarial Gradient Integration (Pan et al., 2021), Expected Gradients (EG) (Erion et al., 2021), Guided Integrated Gradients (GIG) (Kapishnikov et al., 2021) and BlurIG (Xu et al., 2020). Path attribution typically relies on a baseline – a "vanilla" image devoid of features; a path—an often linear path from the featureless baseline to the target image—along which the path integral is computed for every pixel. Granular control over the attribution process comes with difficulties of defining an unambiguously featureless baseline (for each (model, image) pair) (Sturmfels et al., 2020) and then defining a reliable path of increasing label confidence without intermediate inflection points (Akhtar & Jalwana, 2023). To measure the discriminativeness of features identified by attribution methods, experimental benchmarks such as ROAR (Hooker et al., 2019), DiffRAOR (Shah et al., 2021), RISE (Petsiuk et al., 2018) and the Pointing Game (Zhang et al., 2018) have been proposed.

7 Conclusion

In this work, we formally discuss the limitations of current path-attribution frameworks, outline a new principle for optimising baseline and path features, as well as introduce the `UNI` algorithm for unlearning-based neural interpretations. We empirically show that present reliance on static baselines imposes undesirable post-hoc biases which are alien to the model's decision function. We account for and mitigate various infidelity, inconsistency and instability issues in path-attribution by defining principled baselines and conformant path features. `UNI` leverages insights from unlearning to eliminate task-salient features and mimic baseline activations in the "absence of signal". It discovers low-curvature, stable paths with monotonically increasing output confidence, which preserves the completeness axiom necessary for path attribution. We visually, numerically and formally establish the utility of `UNI` as a means to compute robust, meaningful and debiased image attributions. Future extensions to `UNI` include going beyond first-order approximate unlearning towards adopting certified, second-order machine learning techniques; as well as granular investigations on how the baseline definition and model's robustness and inductive biases exert influence on path attribution results.

8 Acknowledgements

References

Josh Achiam, Steven Adler, Sandhini Agarwal, Lama Ahmad, Ilge Akkaya, Florencia Leoni Aleman, Diogo Almeida, Janko Altenschmidt, Sam Altman, Shyamal Anadkat, et al. Gpt-4 technical report. *arXiv preprint arXiv:2303.08774*, 2023. (Cited on page 1.)

Julius Adebayo, Justin Gilmer, Michael Muelly, Ian Goodfellow, Moritz Hardt, and Been Kim. Sanity checks for saliency maps. In S. Bengio, H. Wallach, H. Larochelle, K. Grauman, N. Cesa-Bianchi, and R. Garnett (eds.), *NeurIPS*, volume 31. Curran Associates, Inc., 2018. URL https://proceedings.neurips.cc/paper_files/paper/2018/file/294a8ed24b1ad22ec2e7efea049b8737-Paper.pdf. (Cited on page 2.)

Naveed Akhtar and Mohammad A. A. K. Jalwana. Towards credible visual model interpretation with path attribution. In Andreas Krause, Emma Brunskill, Kyunghyun Cho, Barbara Engelhardt, Sivan Sabato, and Jonathan Scarlett (eds.), *Proceedings of the 40th International Conference on Machine Learning*, volume 202 of *Proceedings of Machine Learning Research*, pp. 439–457. PMLR, 23–29 Jul 2023. URL https://proceedings.mlr.press/v202/akhtar23a.html. (Cited on pages 2, 4, 6, and 9.)

David Alvarez Melis and Tommi Jaakkola. Towards robust interpretability with self-explaining neural networks. *NeurIPS*, 31, 2018. (Cited on page 1.)

Marco Ancona, Enea Ceolini, Cengiz Öztireli, and Markus Gross. Towards better understanding of gradient-based attribution methods for deep neural networks. In *ICLR*, 2018. URL https://openreview.net/forum?id=Sy21R9JAW. (Cited on page 2.)

Anthropic. Introducing the next generation of claude. Mar 2024. URL https://www.anthropic.com/news/claude-3-family. (Cited on page 1.)

Pepa Atanasova, Jakob Grue Simonsen, Christina Lioma, and Isabelle Augenstein. A diagnostic study of explainability techniques for text classification. In *Proceedings of the 2020 Conference on Empirical Methods in Natural Language Processing (EMNLP)*, pp. 3256–3274, 2020. (Cited on page 1.)

David Baehrens, Timon Schroeter, Stefan Harmeling, Motoaki Kawanabe, Katja Hansen, and Klaus-Robert Müller. How to explain individual classification decisions. *Journal of Machine Learning Research*, 11(61):1803–1831, 2010. URL http://jmlr.org/papers/v11/baehrens10a.html. (Cited on page 3.)

David Bau, Bolei Zhou, Aditya Khosla, Aude Oliva, and Antonio Torralba. Network dissection: Quantifying interpretability of deep visual representations. In *Proceedings of the IEEE conference on computer vision and pattern recognition*, pp. 6541–6549, 2017. (Cited on page 1.)

Yoshua Bengio, Geoffrey Hinton, Andrew Yao, Dawn Song, Pieter Abbeel, Yuval Noah Harari, Ya-Qin Zhang, Lan Xue, Shai Shalev-Shwartz, Gillian Hadfield, et al. Managing ai risks in an era of rapid progress. *arXiv preprint arXiv:2310.17688*, 2023. (Cited on page 1.)

Peter Bevan and Amir Atapour-Abarghouei. Skin deep unlearning: Artefact and instrument debiasing in the context of melanoma classification. In *International Conference on Machine Learning*, pp. 1874–1892. PMLR, 2022. (Cited on page 8.)

Umang Bhatt, Adrian Weller, and José MF Moura. Evaluating and aggregating feature-based model explanations. In *Proceedings of the Twenty-Ninth International Conference on International Joint Conferences on Artificial Intelligence*, pp. 3016–3022, 2021. (Cited on pages 1 and 7.)

Moritz Bohle, Mario Fritz, and Bernt Schiele. Convolutional dynamic alignment networks for interpretable classifications. In *Proceedings of the IEEE/CVF Conference on Computer Vision and Pattern Recognition (CVPR)*, pp. 10029–10038, June 2021. (Cited on page 1.)

Moritz Böhle, Mario Fritz, and Bernt Schiele. B-cos networks: Alignment is all we need for interpretability. In *Proceedings of the IEEE/CVF Conference on Computer Vision and Pattern Recognition*, pp. 10329–10338, 2022. (Cited on page 1.)

Sebastian Bordt, Michèle Finck, Eric Raidl, and Ulrike von Luxburg. Post-hoc explanations fail to achieve their purpose in adversarial contexts. In *Proceedings of the 2022 ACM Conference on Fairness, Accountability, and Transparency*, FAccT '22, pp. 891–905, New York, NY, USA, 2022. Association for Computing Machinery. ISBN 9781450393522. doi: 10.1145/3531146.3533153. URL https://doi.org/10.1145/3531146.3533153. (Cited on page 9.)

Lucas Bourtoule, Varun Chandrasekaran, Christopher A Choquette-Choo, Hengrui Jia, Adelin Travers, Baiwu Zhang, David Lie, and Nicolas Papernot. Machine unlearning. In *2021 IEEE Symposium on Security and Privacy (SP)*, pp. 141–159. IEEE Computer Society, 2021. (Cited on page 8.)

Wieland Brendel and Matthias Bethge. Approximating cnns with bag-of-local-features models works surprisingly well on imagenet. In *International Conference on Learning Representations*, 2018. (Cited on page 1.)

Tim Brooks, Bill Peebles, Connor Holmes, Will DePue, Yufei Guo, Li Jing, David Schnurr, Joe Taylor, Troy Luhman, Eric Luhman, Clarence Ng, Ricky Wang, and Aditya Ramesh. Video generation models as world simulators. 2024. URL https://openai.com/research/video-generation-models-as-world-simulators. (Cited on page 1.)

Jonathan Brophy and Daniel Lowd. Machine unlearning for random forests. In *International Conference on Machine Learning*, pp. 1092–1104. PMLR, 2021. (Cited on page 8.)

Siu Lun Chau, Robert Hu, Javier Gonzalez, and Dino Sejdinovic. RKHS-SHAP: Shapley values for kernel methods. In Alice H. Oh, Alekh Agarwal, Danielle Belgrave, and Kyunghyun Cho (eds.), *Advances in Neural Information Processing Systems*, 2022. URL https://openreview.net/forum?id=gnc2VJHXmsG. (Cited on page 9.)

Chaofan Chen, Oscar Li, Daniel Tao, Alina Barnett, Cynthia Rudin, and Jonathan K Su. This looks like that: Deep learning for interpretable image recognition. In H. Wallach, H. Larochelle, A. Beygelzimer, F. d'Alché-Buc, E. Fox, and R. Garnett (eds.), *Advances in Neural Information Processing Systems*, volume 32. Curran Associates, Inc., 2019. URL https://proceedings.neurips.cc/paper_files/paper/2019/file/adf7ee2dcf142b0e11888e72b43fcb75-Paper.pdf. (Cited on page 1.)

Ruizhe Chen, Jianfei Yang, Huimin Xiong, Jianhong Bai, Tianxiang Hu, Jin Hao, Yang Feng, Joey Tianyi Zhou, Jian Wu, and Zuozhu Liu. Fast model debias with machine unlearning. *Advances in Neural Information Processing Systems*, 36, 2024. (Cited on page 8.)

Ching Lam Choi and Farzan Farnia. On the generalization of gradient-based neural network interpretations, 2024. URL https://openreview.net/forum?id=EwAGztBkJ6. (Cited on page 9.)

Google Deepmind. Veo: Our most capable generative video model. May 2024. URL https://deepmind.google/technologies/veo/. (Cited on page 1.)

Jia Deng, Wei Dong, Richard Socher, Li-Jia Li, Kai Li, and Li Fei-Fei. Imagenet: A large-scale hierarchical image database. In *CVPR*, pp. 248–255, 2009. doi: 10.1109/CVPR.2009.5206848. (Cited on page 6.)

Ann-Kathrin Dombrowski, Maximillian Alber, Christopher Anders, Marcel Ackermann, Klaus-Robert Müller, and Pan Kessel. Explanations can be manipulated and geometry is to blame. *Advances in neural information processing systems*, 32, 2019. (Cited on pages 2 and 6.)

Finale Doshi-Velez and Been Kim. Towards a rigorous science of interpretable machine learning. *arXiv preprint arXiv:1702.08608*, 2017. (Cited on page 1.)

Alexey Dosovitskiy, Lucas Beyer, Alexander Kolesnikov, Dirk Weissenborn, Xiaohua Zhai, Thomas Unterthiner, Mostafa Dehghani, Matthias Minderer, Georg Heigold, Sylvain Gelly, et al. An image is worth 16x16 words: Transformers for image recognition at scale. In *International Conference on Learning Representations*, 2020. (Cited on page 6.)

Cynthia Dwork. *Differential Privacy*, pp. 338–340. Springer US, Boston, MA, 2011. ISBN 978-1-4419-5906-5. doi: 10.1007/978-1-4419-5906-5_752. URL https://doi.org/10.1007/978-1-4419-5906-5_752. (Cited on page 8.)

Dumitru Erhan, Yoshua Bengio, Aaron Courville, and Pascal Vincent. Visualizing higher-layer features of a deep network. 2009. (Cited on pages 3 and 9.)

Gabriel Erion, Joseph D Janizek, Pascal Sturmfels, Scott M Lundberg, and Su-In Lee. Improving performance of deep learning models with axiomatic attribution priors and expected gradients. *Nature machine intelligence*, 3(7):620–631, 2021. (Cited on pages 2 and 9.)

European Commission. Laying down harmonised rules on artificial intelligence (artificial intelligence act) and amending certain union legislative acts. *CNECT*, Apr 2021. URL https://digital-strategy.ec.europa.eu/en/library/proposal-regulation-laying-down-harmonised-rules-artificial-intelligence. (Cited on page 1.)

Thomas Fel, David Vigouroux, Rémi Cadène, and Thomas Serre. How good is your explanation? algorithmic stability measures to assess the quality of explanations for deep neural networks. In *Proceedings of the IEEE/CVF Winter Conference on Applications of Computer Vision*, pp. 720–730, 2022. (Cited on page 9.)

Eric J. Friedman. Paths and consistency in additive cost sharing. *Int. J. Game Theory*, 32(4):501–518, aug 2004. ISSN 0020-7276. doi: 10.1007/s001820400173. URL https://doi.org/10.1007/s001820400173. (Cited on page 9.)

Amirata Ghorbani, Abubakar Abid, and James Zou. Interpretation of neural networks is fragile. In *AAAI*, volume 33, pp. 3681–3688, 2019a. (Cited on pages 2 and 7.)

Amirata Ghorbani, James Wexler, James Y Zou, and Been Kim. Towards automatic concept-based explanations. In H. Wallach, H. Larochelle, A. Beygelzimer, F. d'Alché-Buc, E. Fox, and R. Garnett (eds.), *NeurIPS*, volume 32, 2019b. URL https://proceedings.neurips.cc/paper_files/paper/2019/file/77d2afcb31f6493e350fca61764efb9a-Paper.pdf. (Cited on page 1.)

Antonio Ginart, Melody Guan, Gregory Valiant, and James Y Zou. Making ai forget you: Data deletion in machine learning. *Advances in neural information processing systems*, 32, 2019. (Cited on page 8.)

Aditya Golatkar, Alessandro Achille, and Stefano Soatto. Eternal sunshine of the spotless net: Selective forgetting in deep networks. In *Proceedings of the IEEE/CVF Conference on Computer Vision and Pattern Recognition*, pp. 9304–9312, 2020. (Cited on page 8.)

Ian J Goodfellow, Jonathon Shlens, and Christian Szegedy. Explaining and harnessing adversarial examples. *arXiv preprint arXiv:1412.6572*, 2014. (Cited on pages 2 and 7.)

Google. Introducing paligemma, gemma 2, and an upgraded responsible ai toolkit. May 2024. URL https://developers.googleblog.com/en/gemma-family-and-toolkit-expansion-io-2024/. (Cited on page 1.)

Chuan Guo, Tom Goldstein, Awni Hannun, and Laurens Van Der Maaten. Certified data removal from machine learning models. In *Proceedings of the 37th International Conference on Machine Learning*, pp. 3832–3842, 2020. (Cited on page 8.)

Kaiming He, Xiangyu Zhang, Shaoqing Ren, and Jian Sun. Deep residual learning for image recognition. In *Proceedings of the IEEE conference on computer vision and pattern recognition*, pp. 770–778, 2016. (Cited on page 6.)

Dan Hendrycks and Thomas Dietterich. Benchmarking neural network robustness to common corruptions and perturbations. In *International Conference on Learning Representations*, 2019. (Cited on pages 4 and 6.)

Sara Hooker, Dumitru Erhan, Pieter-Jan Kindermans, and Been Kim. A benchmark for interpretability methods in deep neural networks. *NeurIPS*, 32, 2019. (Cited on page 9.)

Dominik Janzing, Lenon Minorics, and Patrick Bloebaum. Feature relevance quantification in explainable ai: A causal problem. In *Proceedings of the Twenty Third International Conference on Artificial Intelligence and Statistics*, volume 108 of *Proceedings of Machine Learning Research*, pp. 2907–2916. PMLR, 26–28 Aug 2020. URL https://proceedings.mlr.press/v108/janzing20a.html. (Cited on page 9.)

Albert Q Jiang, Alexandre Sablayrolles, Arthur Mensch, Chris Bamford, Devendra Singh Chaplot, Diego de las Casas, Florian Bressand, Gianna Lengyel, Guillaume Lample, Lucile Saulnier, et al. Mistral 7b. *arXiv preprint arXiv:2310.06825*, 2023. (Cited on page 1.)

Andrei Kapishnikov, Subhashini Venugopalan, Besim Avci, Ben Wedin, Michael Terry, and Tolga Bolukbasi. Guided integrated gradients: An adaptive path method for removing noise. In *CVPR*, pp. 5050–5058, 2021. (Cited on pages 2, 6, and 9.)

Been Kim, Martin Wattenberg, Justin Gilmer, Carrie Cai, James Wexler, Fernanda Viegas, et al. Interpretability beyond feature attribution: Quantitative testing with concept activation vectors (tcav). In *International conference on machine learning*, pp. 2668–2677. PMLR, 2018. (Cited on page 1.)

Byungju Kim, Hyunwoo Kim, Kyungsu Kim, Sungjin Kim, and Junmo Kim. Learning not to learn: Training deep neural networks with biased data. In *Proceedings of the IEEE/CVF conference on computer vision and pattern recognition*, pp. 9012–9020, 2019. (Cited on page 8.)

Pang Wei Koh, Thao Nguyen, Yew Siang Tang, Stephen Mussmann, Emma Pierson, Been Kim, and Percy Liang. Concept bottleneck models. In Hal Daumé III and Aarti Singh (eds.), *Proceedings of the 37th International Conference on Machine Learning*, volume 119 of *Proceedings of Machine Learning Research*, pp. 5338–5348. PMLR, 13–18 Jul 2020. URL https://proceedings.mlr.press/v119/koh20a.html. (Cited on page 1.)

Ramaravind Kommiya Mothilal, Divyat Mahajan, Chenhao Tan, and Amit Sharma. Towards unifying feature attribution and counterfactual explanations: Different means to the same end. In *Proceedings of the 2021 AAAI/ACM Conference on AI, Ethics, and Society*, AIES '21, pp. 652–663. Association for Computing Machinery, 2021. ISBN 9781450384735. doi: 10.1145/3461702.3462597. URL https://doi.org/10.1145/3461702.3462597. (Cited on page 9.)

Haotian Liu, Chunyuan Li, Qingyang Wu, and Yong Jae Lee. Visual instruction tuning. In *NeurIPS*, 2023. URL https://openreview.net/forum?id=w0H2xGHlkw. (Cited on page 1.)

Ze Liu, Yutong Lin, Yue Cao, Han Hu, Yixuan Wei, Zheng Zhang, Stephen Lin, and Baining Guo. Swin transformer: Hierarchical vision transformer using shifted windows. In *Proceedings of the IEEE/CVF international conference on computer vision*, pp. 10012–10022, 2021. (Cited on page 6.)

Zhuang Liu, Hanzi Mao, Chao-Yuan Wu, Christoph Feichtenhofer, Trevor Darrell, and Saining Xie. A convnet for the 2020s. In *Proceedings of the IEEE/CVF conference on computer vision and pattern recognition*, pp. 11976–11986, 2022. (Cited on page 6.)

Scott M. Lundberg, Gabriel Erion, Hugh Chen, Alex DeGrave, Jordan M. Prutkin, Bala Nair, Ronit Katz, Jonathan Himmelfarb, Nisha Bansal, and Su-In Lee. From local explanations to global understanding with explainable ai for trees. *Nature machine intelligence*, 2. doi: 10.1038/s42256-019-0138-9. URL https://par.nsf.gov/biblio/10167481. (Cited on page 9.)

Meta. Introducing meta llama 3: The most capable openly available llm to date. Apr 2024. URL https://ai.meta.com/blog/meta-llama-3/. (Cited on page 1.)

Grégoire Montavon, Alexander Binder, Sebastian Lapuschkin, Wojciech Samek, and Klaus-Robert Müller. *Layer-Wise Relevance Propagation: An Overview*, pp. 193–209. Springer International Publishing, Cham, 2019. ISBN 978-3-030-28954-6. doi: 10.1007/978-3-030-28954-6_10. URL https://doi.org/10.1007/978-3-030-28954-6_10. (Cited on page 9.)

Thanh Tam Nguyen, Thanh Trung Huynh, Phi Le Nguyen, Alan Wee-Chung Liew, Hongzhi Yin, and Quoc Viet Hung Nguyen. A survey of machine unlearning. *arXiv preprint arXiv:2209.02299*, 2022. (Cited on page 8.)

Deng Pan, Xin Li, and Dongxiao Zhu. Explaining deep neural network models with adversarial gradient integration. In *IJCAI*, pp. 2876–2883. International Joint Conferences on Artificial Intelligence Organization, 8 2021. doi: 10.24963/ijcai.2021/396. URL https://doi.org/10.24963/ijcai.2021/396. Main Track. (Cited on pages 6 and 9.)

Adam Paszke, Sam Gross, Francisco Massa, Adam Lerer, James Bradbury, Gregory Chanan, Trevor Killeen, Zeming Lin, Natalia Gimelshein, Luca Antiga, Alban Desmaison, Andreas Kopf, Edward Yang, Zachary DeVito, Martin Raison, Alykhan Tejani, Sasank Chilamkurthy, Benoit Steiner, Lu Fang, Junjie Bai, and Soumith Chintala. Pytorch: An imperative style, high-performance deep learning library. In *Advances in Neural Information Processing Systems 32*, pp. 8024–8035. Curran Associates, Inc., 2019. URL http://papers.neurips.cc/paper/9015-pytorch-an-imperative-style-high-performance-deep-learning-library.pdf. (Cited on page 6.)

Vitali Petsiuk, Abir Das, and Kate Saenko. RISE: randomized input sampling for explanation of black-box models. In *BMVC*, pp. 151. BMVA Press, 2018. URL http://bmvc2018.org/contents/papers/1064.pdf. (Cited on page 9.)

Marco Tulio Ribeiro, Sameer Singh, and Carlos Guestrin. "why should i trust you?": Explaining the predictions of any classifier. In *Proceedings of the 22nd ACM SIGKDD International Conference on Knowledge Discovery and Data Mining*, KDD '16, pp. 1135–1144, New York, NY, USA, 2016. Association for Computing Machinery. ISBN 9781450342322. doi: 10.1145/2939672.2939778. URL https://doi.org/10.1145/2939672.2939778. (Cited on page 9.)

Robin Rombach, Andreas Blattmann, Dominik Lorenz, Patrick Esser, and Björn Ommer. High-resolution image synthesis with latent diffusion models. In *Proceedings of the IEEE/CVF conference on computer vision and pattern recognition*, pp. 10684–10695, 2022. (Cited on page 1.)

Andrew Slavin Ross, Michael C. Hughes, and Finale Doshi-Velez. Right for the right reasons: Training differentiable models by constraining their explanations. In *Proceedings of the Twenty-Sixth International Joint Conference on Artificial Intelligence, IJCAI-17*, pp. 2662–2670, 2017. doi: 10.24963/ijcai.2017/371. URL https://doi.org/10.24963/ijcai.2017/371. (Cited on page 1.)

D. Sculley, Gary Holt, Daniel Golovin, Eugene Davydov, Todd Phillips, Dietmar Ebner, Vinay Chaudhary, Michael Young, Jean-François Crespo, and Dan Dennison. Hidden technical debt in machine learning systems. In C. Cortes, N. Lawrence, D. Lee, M. Sugiyama, and R. Garnett (eds.), *Advances in Neural Information Processing Systems*, volume 28. Curran Associates, Inc., 2015. URL https://proceedings.neurips.cc/paper_files/paper/2015/file/86df7dcfd896fcaf2674f757a2463eba-Paper.pdf. (Cited on page 9.)

Ramprasaath R Selvaraju, Michael Cogswell, Abhishek Das, Ramakrishna Vedantam, Devi Parikh, and Dhruv Batra. Grad-cam: Visual explanations from deep networks via gradient-based localization. In *CVPR*, pp. 618–626, 2017. (Cited on page 9.)

Harshay Shah, Prateek Jain, and Praneeth Netrapalli. Do input gradients highlight discriminative features? *Advances in Neural Information Processing Systems*, 34:2046–2059, 2021. (Cited on page 9.)

Avanti Shrikumar, Peyton Greenside, Anna Shcherbina, and Anshul Kundaje. Not just a black box: Learning important features through propagating activation differences. *arXiv preprint arXiv:1605.01713*, 2016. (Cited on pages 2, 3, 6, and 9.)

K Simonyan and A Zisserman. Very deep convolutional networks for large-scale image recognition. In *3rd International Conference on Learning Representations (ICLR 2015)*, 2015. (Cited on page 6.)

Karen Simonyan, Andrea Vedaldi, and Andrew Zisserman. Deep inside convolutional networks: Visualising image classification models and saliency maps. *arXiv preprint arXiv:1312.6034*, 2013. (Cited on pages 3 and 9.)

Daniel Smilkov, Nikhil Thorat, Been Kim, Fernanda Viégas, and Martin Wattenberg. Smoothgrad: removing noise by adding noise. *arXiv preprint arXiv:1706.03825*, 2017. (Cited on pages 2 and 9.)

Jost Tobias Springenberg, Alexey Dosovitskiy, Thomas Brox, and Martin Riedmiller. Striving for simplicity: The all convolutional net. *arXiv preprint arXiv:1412.6806*, 2014. (Cited on pages 6 and 9.)

Suraj Srinivas and Francois Fleuret. Full-gradient representation for neural network visualization, 2019. (Cited on page 6.)

Pascal Sturmfels, Scott Lundberg, and Su-In Lee. Visualizing the impact of feature attribution baselines. *Distill*, 2020. doi: 10.23915/distill.00022. https://distill.pub/2020/attribution-baselines. (Cited on pages 2, 4, and 9.)

Mukund Sundararajan, Ankur Taly, and Qiqi Yan. Gradients of counterfactuals, 2016. (Cited on pages 2 and 3.)

Mukund Sundararajan, Ankur Taly, and Qiqi Yan. Axiomatic attribution for deep networks. In *International conference on machine learning*, pp. 3319–3328. PMLR, 2017. (Cited on pages 2, 3, 6, and 9.)

Mingxing Tan and Quoc Le. Efficientnetv2: Smaller models and faster training. In *International conference on machine learning*, pp. 10096–10106. PMLR, 2021. (Cited on page 6.)

Anvith Thudi, Gabriel Deza, Varun Chandrasekaran, and Nicolas Papernot. Unrolling sgd: Understanding factors influencing machine unlearning. In *2022 IEEE 7th European Symposium on Security and Privacy (EuroS&P)*, pp. 303–319. IEEE, 2022. (Cited on page 8.)

White House OSTP. Blueprint for an ai bill of rights: Making automated systems work for the american people. Oct 2022. URL https://www.whitehouse.gov/wp-content/uploads/2022/10/Blueprint-for-an-AI-Bill-of-Rights.pdf. (Cited on page 1.)

Shawn Xu, Subhashini Venugopalan, and Mukund Sundararajan. Attribution in scale and space. In *CVPR*, June 2020. (Cited on pages 2, 6, and 9.)

Chih-Kuan Yeh, Cheng-Yu Hsieh, Arun Suggala, David I Inouye, and Pradeep K Ravikumar. On the (in) fidelity and sensitivity of explanations. *NeurIPS*, 32, 2019. (Cited on page 1.)

Chih-Kuan Yeh, Been Kim, Sercan Arik, Chun-Liang Li, Tomas Pfister, and Pradeep Ravikumar. On completeness-aware concept-based explanations in deep neural networks. *Advances in neural information processing systems*, 33: 20554–20565, 2020. (Cited on page 9.)

Matthew D Zeiler and Rob Fergus. Visualizing and understanding convolutional networks. In *Computer Vision–ECCV 2014: 13th European Conference, Zurich, Switzerland, September 6-12, 2014, Proceedings, Part I 13*, pp. 818–833. Springer, 2014. (Cited on page 9.)

Jianming Zhang, Sarah Adel Bargal, Zhe Lin, Jonathan Brandt, Xiaohui Shen, and Stan Sclaroff. Top-down neural attention by excitation backprop. *IJCV*, 126(10):1084–1102, 2018. (Cited on page 9.)

Bolei Zhou, Yiyou Sun, David Bau, and Antonio Torralba. Interpretable basis decomposition for visual explanation. In *Proceedings of the European Conference on Computer Vision (ECCV)*, September 2018. (Cited on page 1.)

A Appendix

We supplement the main text with visualisations of the `UNI` baseline, attributions and path features (properties, stability and robustness). We additionally include figures elucidating the colour, texture and frequency biases post-hoc imposed by path attribution methods. From Figure 7, we observe the stability of `UNI` path features: our attributions can be reliably and efficiently computed with Riemann approximation. In Figures 8, 9 and 10, we present visualisations on ImageNet-C, highlighting how static choices of baselines may bias the path-attribution procedure, leading to null or noisy explanations. `UNI` does not impose additional post-hoc assumptions that are alien to the model's decision function. Furthermore, we present qualitative comparisons of attribution results of pre-trained models on the ImageNet-1K test set, in Figures 11, 12, 13, 14, 15 and 16. `UNI` attributions are visibly better localised and more semantically meaningful. Finally, we visualise the consistent, geodesic paths of monotonically increasing output confidence, discovered by `UNI`. As seen from Figures 17, 18, 19, 20, 21 and 22, while other path attribution methods might encounter extrema and turning points along the interpolation path from baseline to input, `UNI`'s path features are monotonic and preserve the crucial completeness property on which the path attribution framework depends.
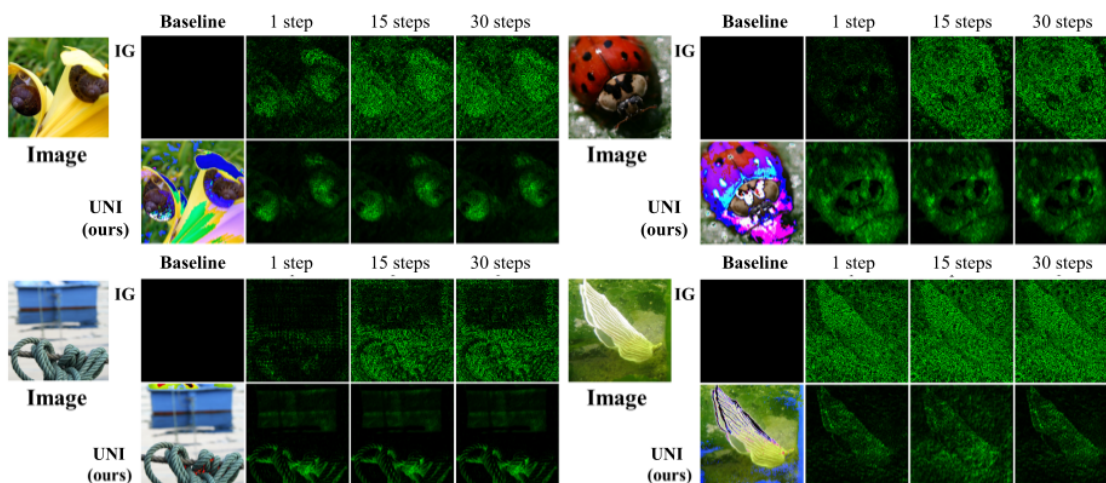
Figure 7: Comparison of attribution maps computed by Integrated Gradients and `UNI`, for a pre-trained ResNet-18 on the ImageNet-1K test set. `UNI` occludes and unlearns predictive input features; reliably localises predictive image regions; can be efficiently computed with only 1 Riemann step.
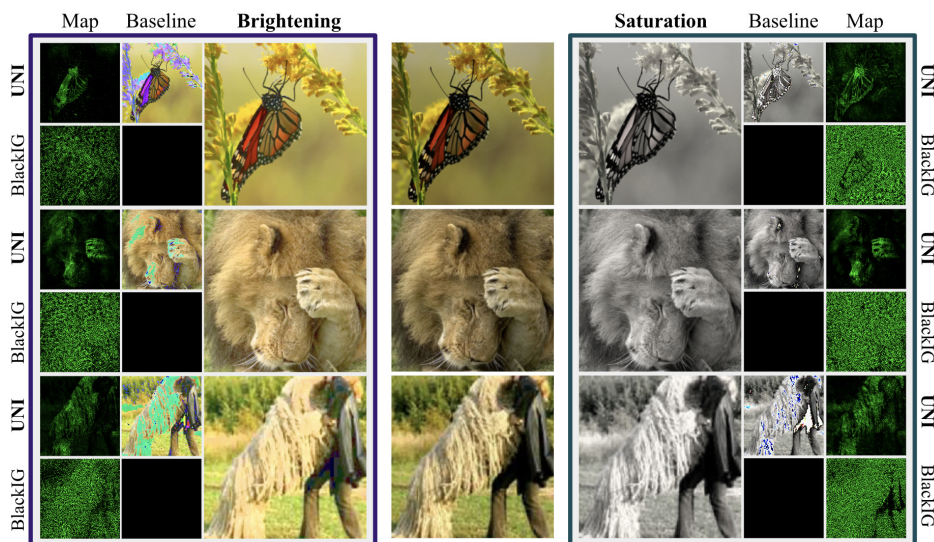
Figure 8: *Colour bias:* When an image's brightness or saturation is altered, IG with a black baseline fails to identify dark features, such as the wings of the butterfly (R1) or black jacket (R3).

16
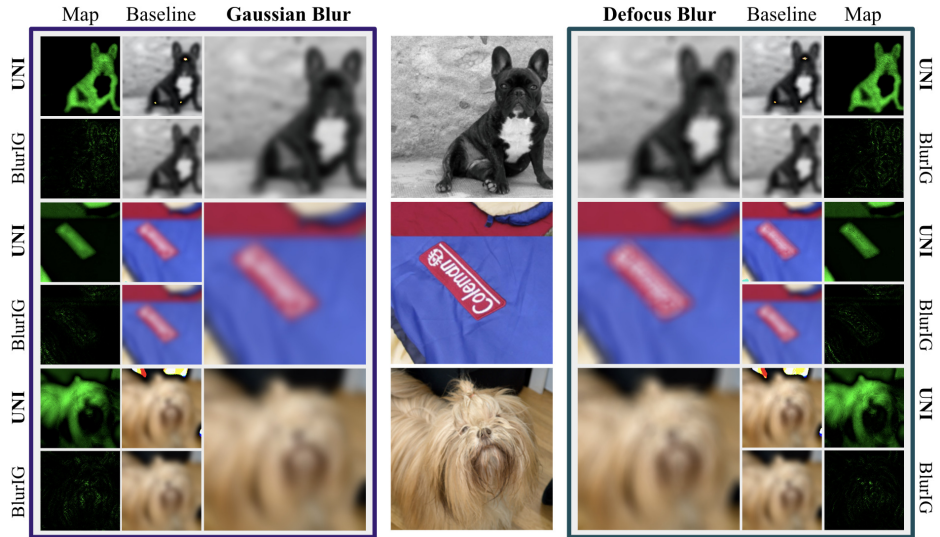
Figure 9: *Texture bias:* Using a blurred baseline for IG leads to a smoothness assumption in image texture, which leads to missingness in attribution when the input is also gaussian or defocus blurred.
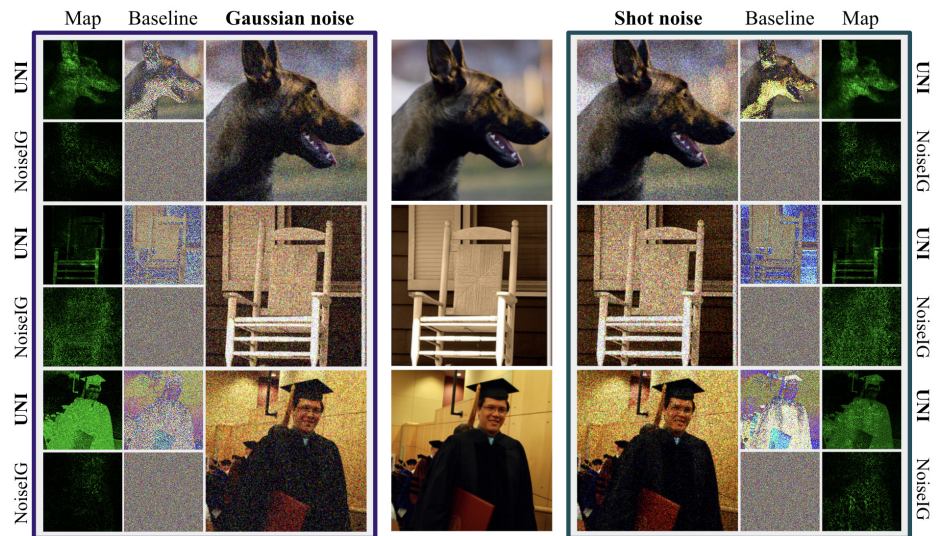

Figure 10: *Frequency bias:* A gaussian noised baseline for IG renders it vulnerable to high-frequency corruptions. Adding gaussian or shot noise to the image yields unmeaningful, noisy attributions.
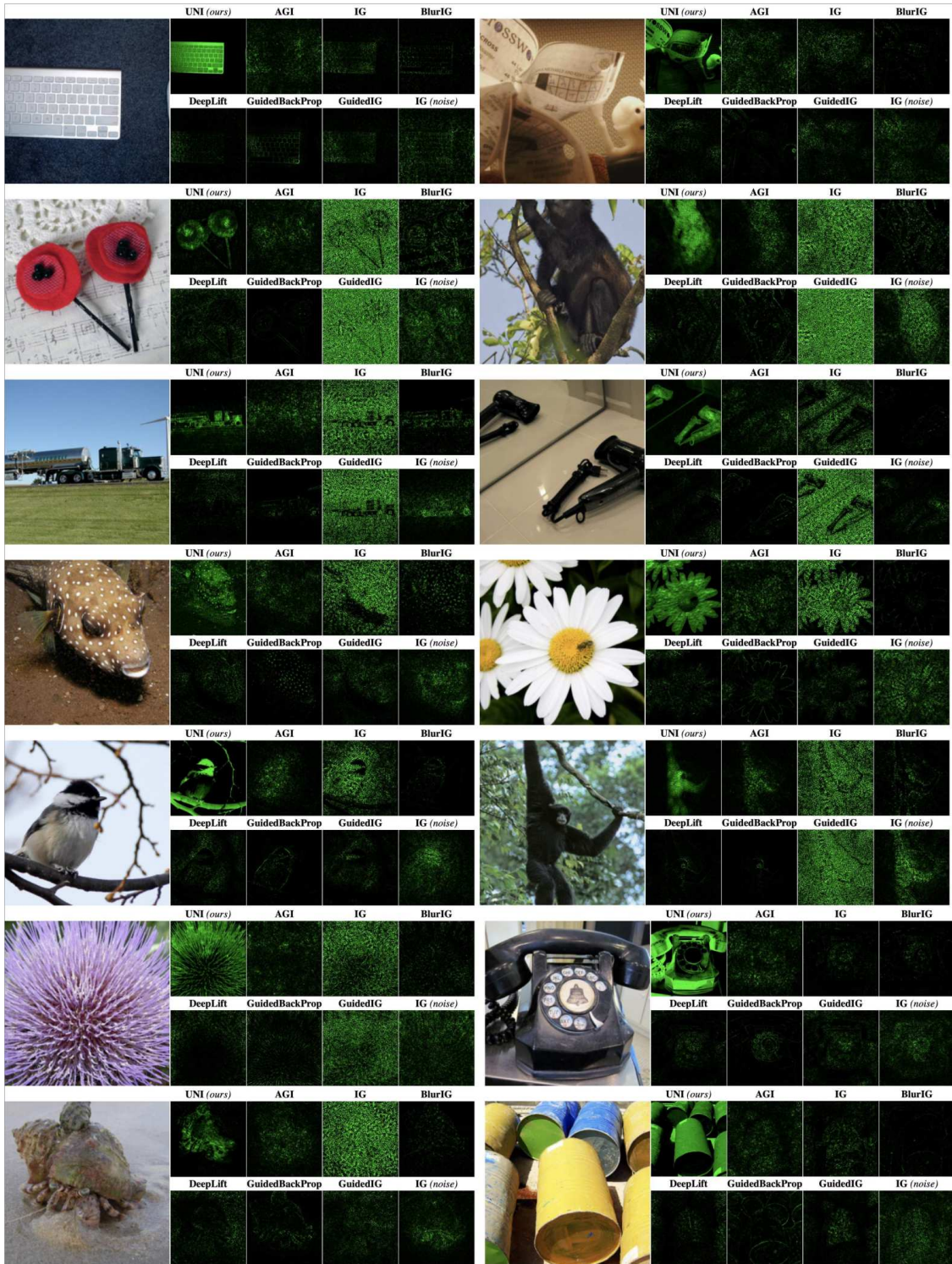
Figure 11: *Comparing attributions (ResNet-18):* UNI attributions demonstrate higher saliency, fidelity and faithfulness relative to conventional baselines on the ImageNet test set.
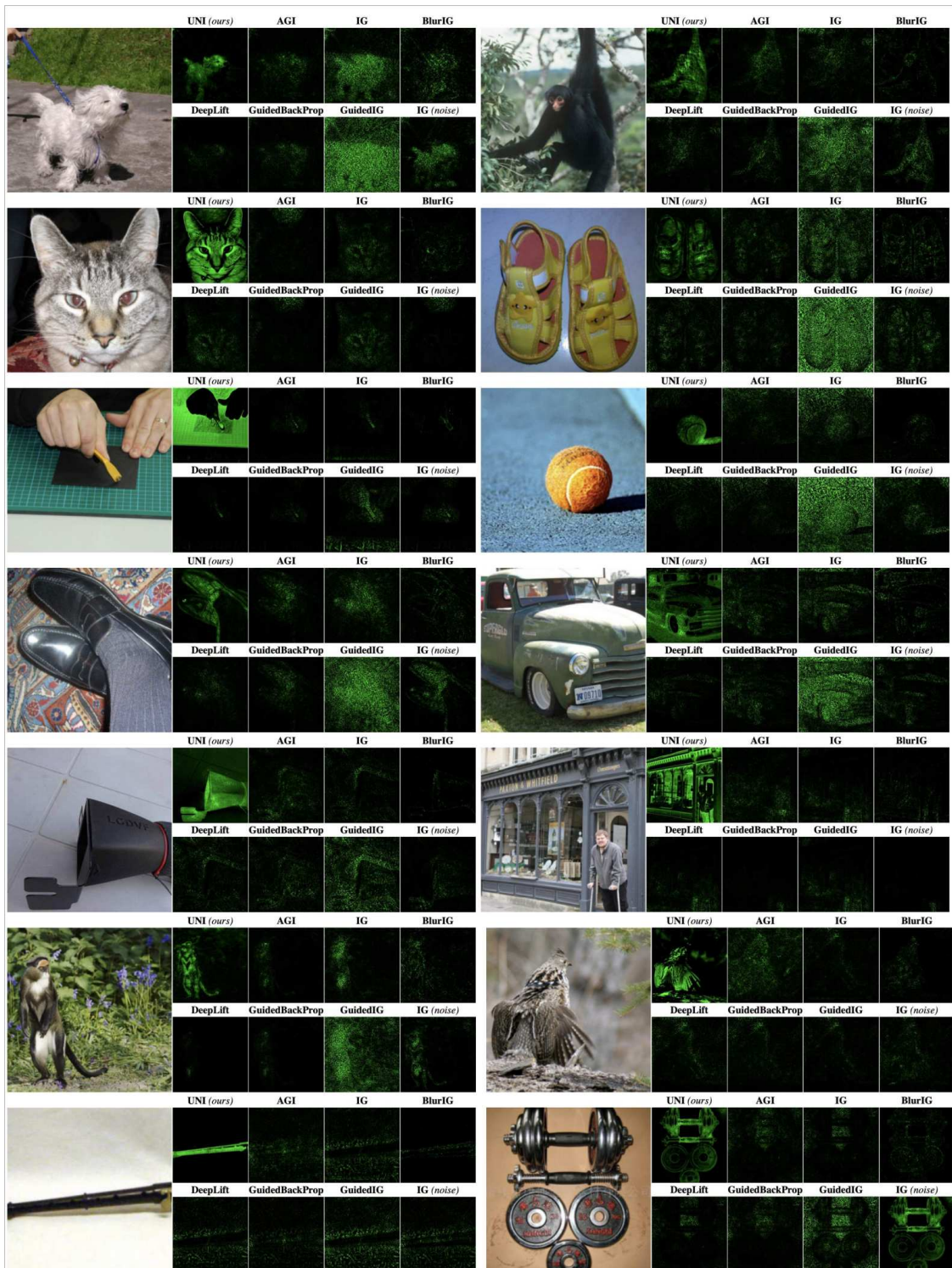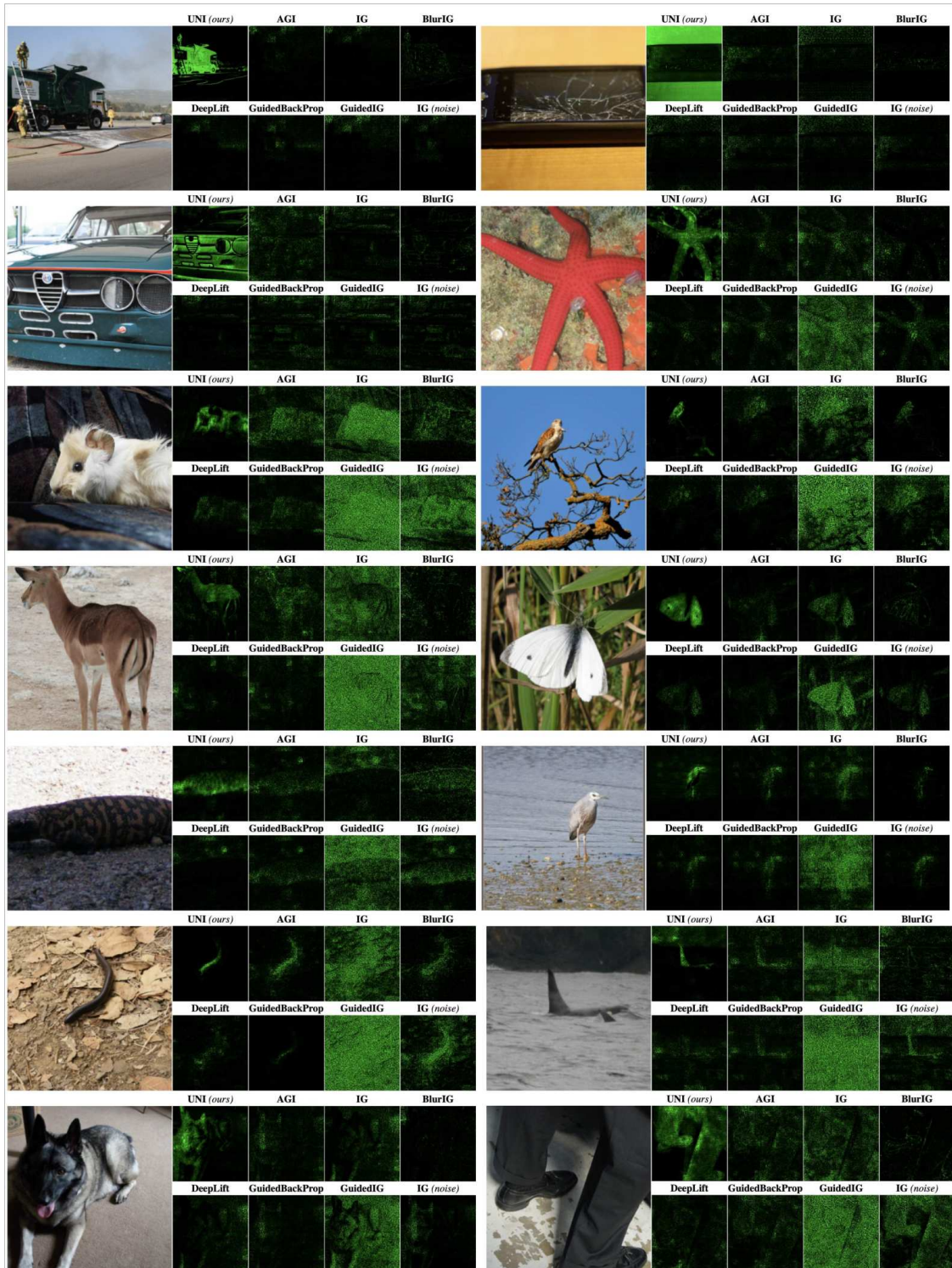
Figure 12: *Comparing attributions (EfficientNet-v2-small):* UNI attributions demonstrate higher saliency, fidelity and faithfulness relative to conventional baselines on the ImageNet test set.
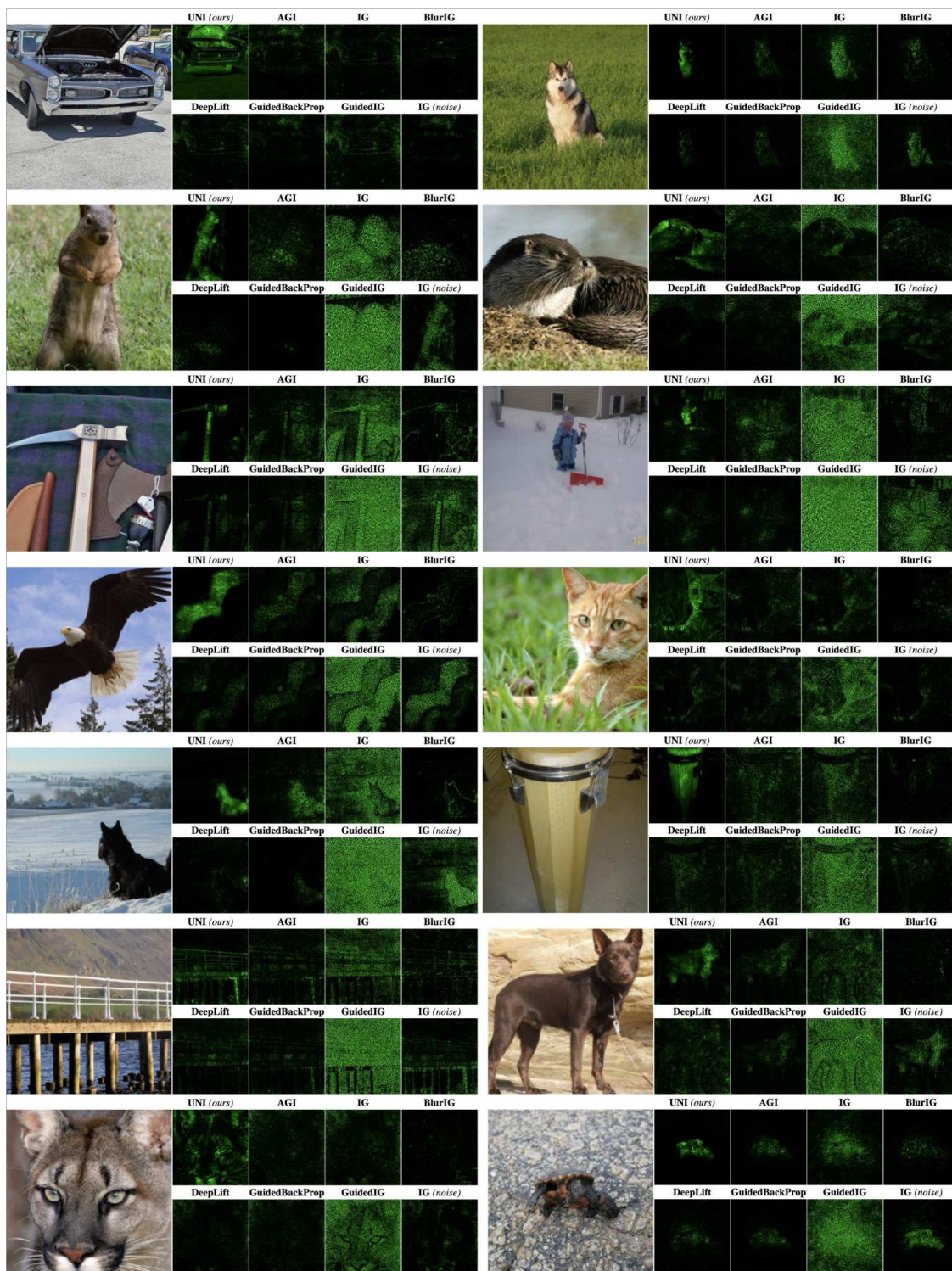
Figure 13: *Comparing attributions (ConvNeXt-Tiny):* UNI attributions demonstrate higher saliency, fidelity and faithfulness relative to conventional baselines on the ImageNet test set.
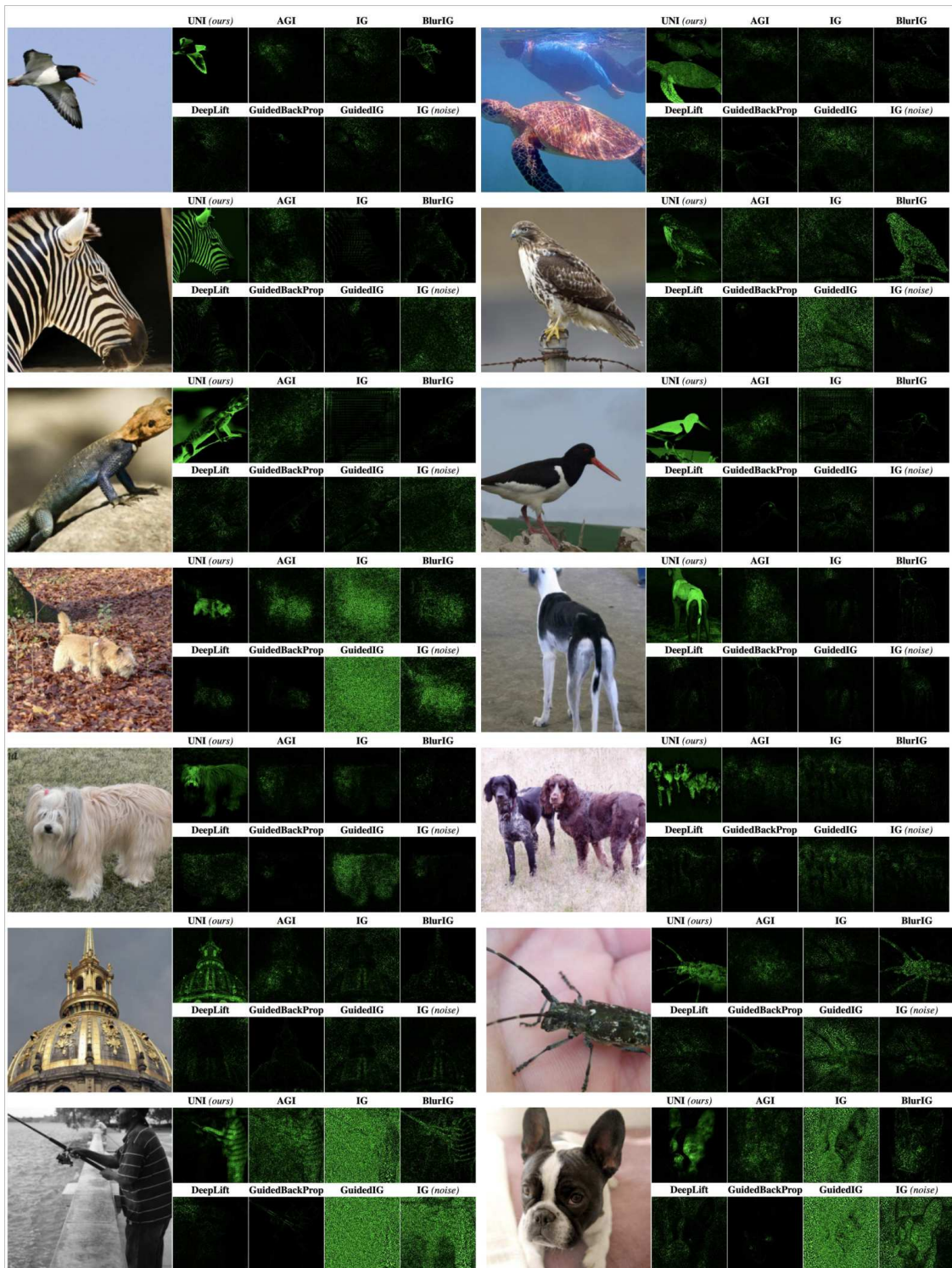
Figure 14: *Comparing attributions (VGG-16-bn):* UNI attributions demonstrate higher saliency, fidelity and faithfulness relative to conventional baselines on the ImageNet test set.
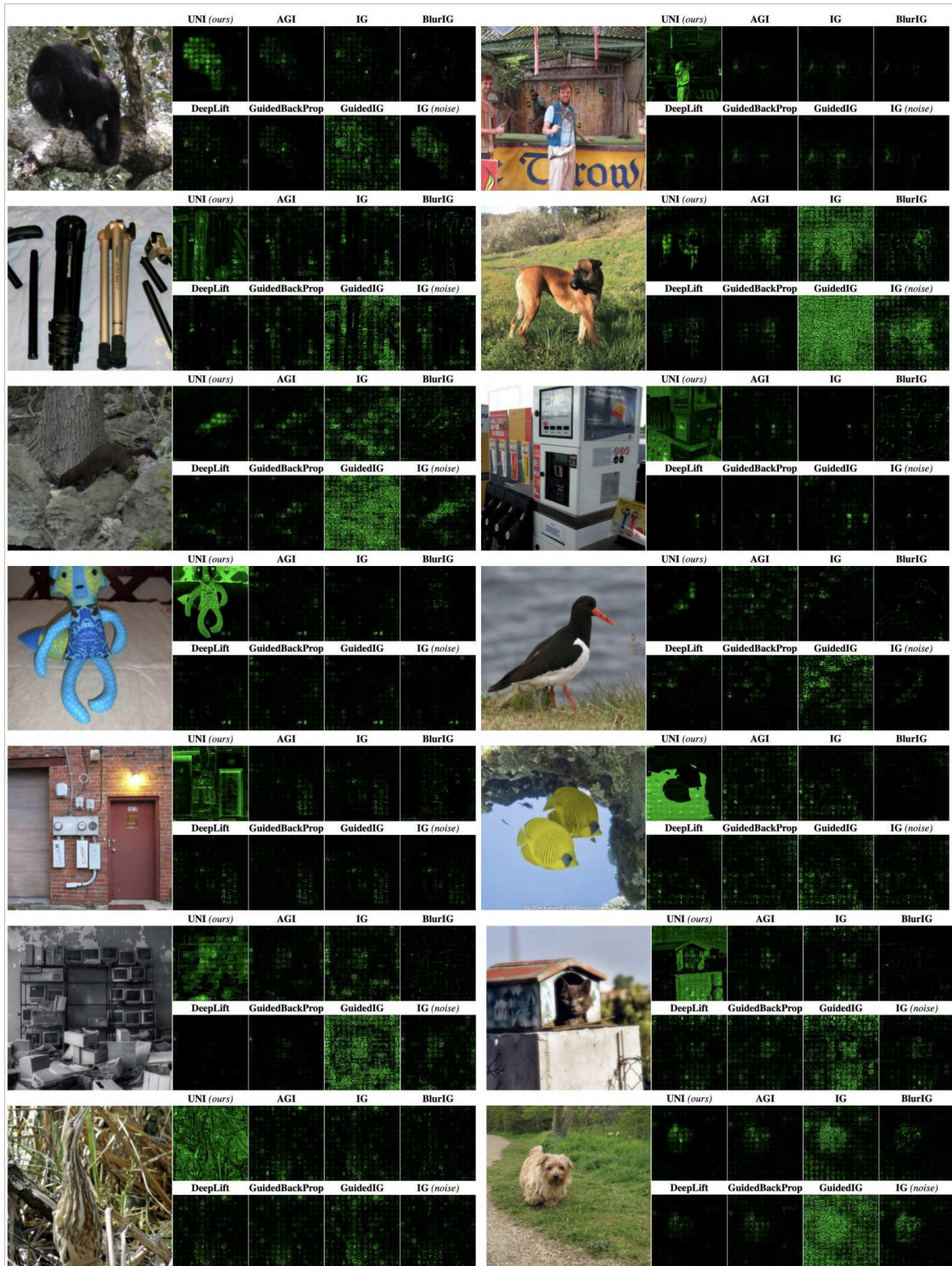
Figure 15: *Comparing attributions (ViT-B_16):* UNI attributions demonstrate higher saliency, fidelity and faithfulness relative to conventional baselines on the ImageNet test set.

Figure 16: *Comparing attributions (Swin-Transformer-Tiny):* `UNI` attributions demonstrate higher saliency, fidelity and faithfulness relative to conventional baselines on the ImageNet test set.
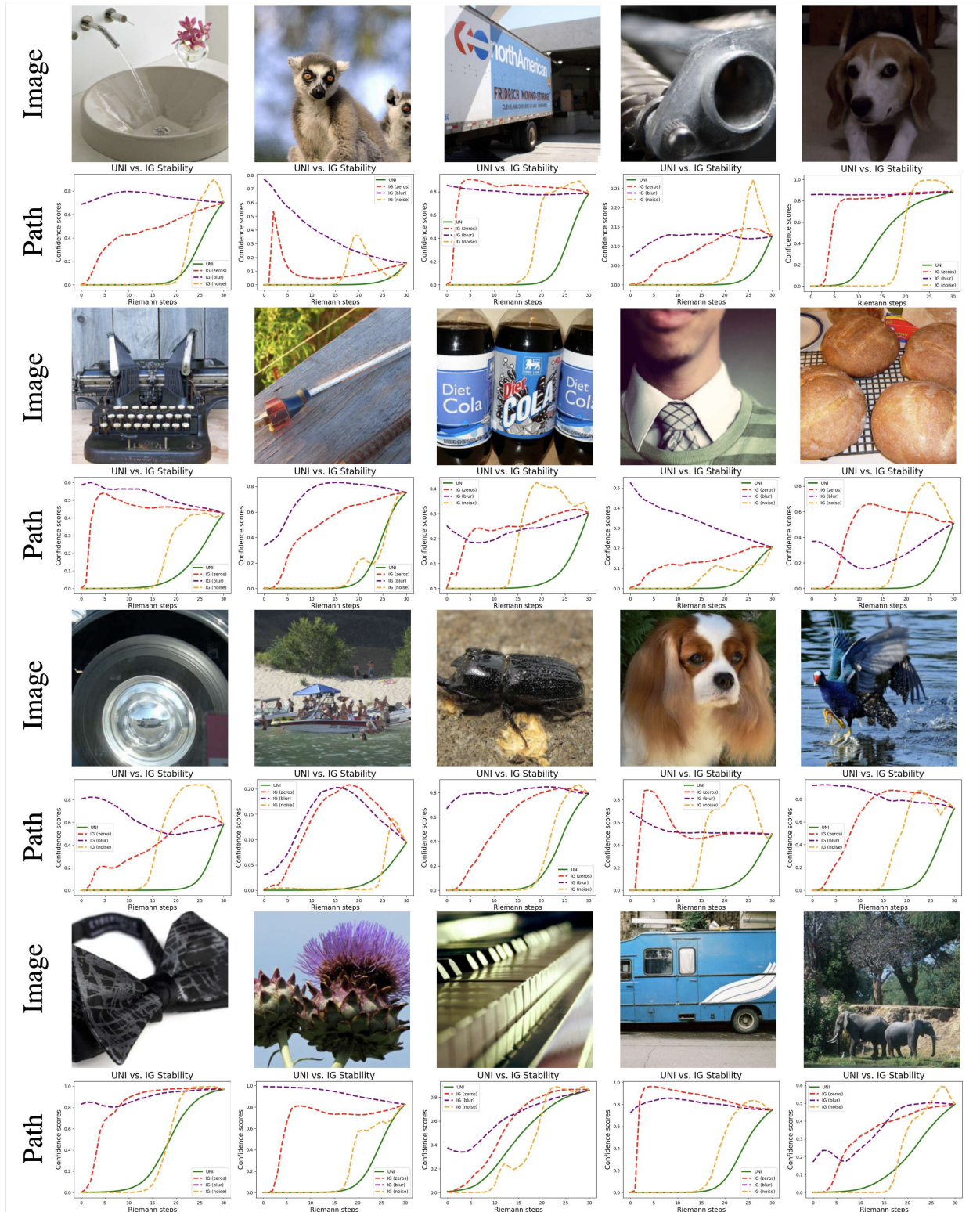
Figure 17: *Comparing paths (ResNet-18):* UNI discovers geodesic paths of monotonically increasing output confidence, preserving the completeness property required for robust attributions.
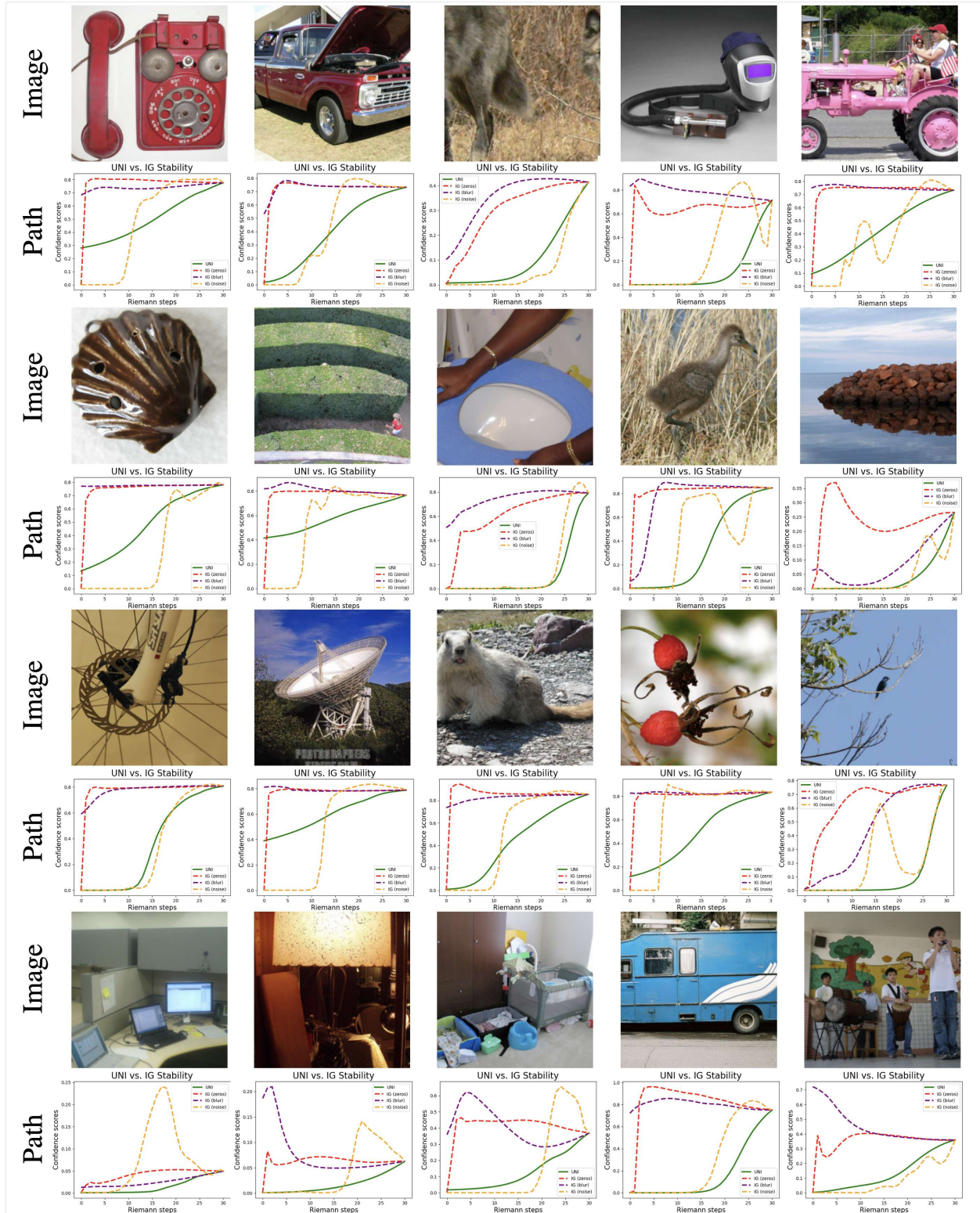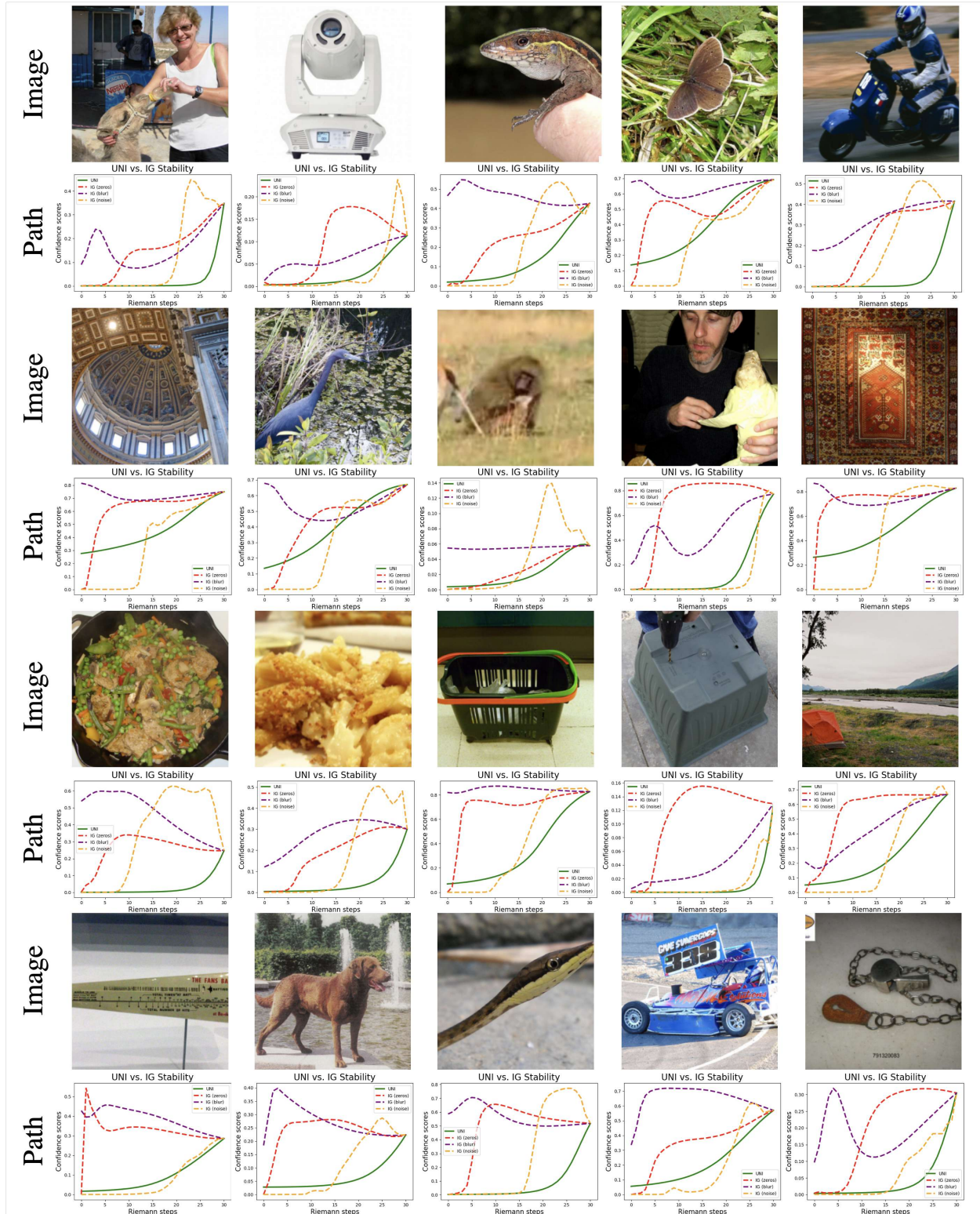
Figure 18: *Comparing paths (EfficientNet-v2-small):* UNI discovers geodesic paths of monotonically increasing output confidence, preserving the completeness property required for robust attributions.
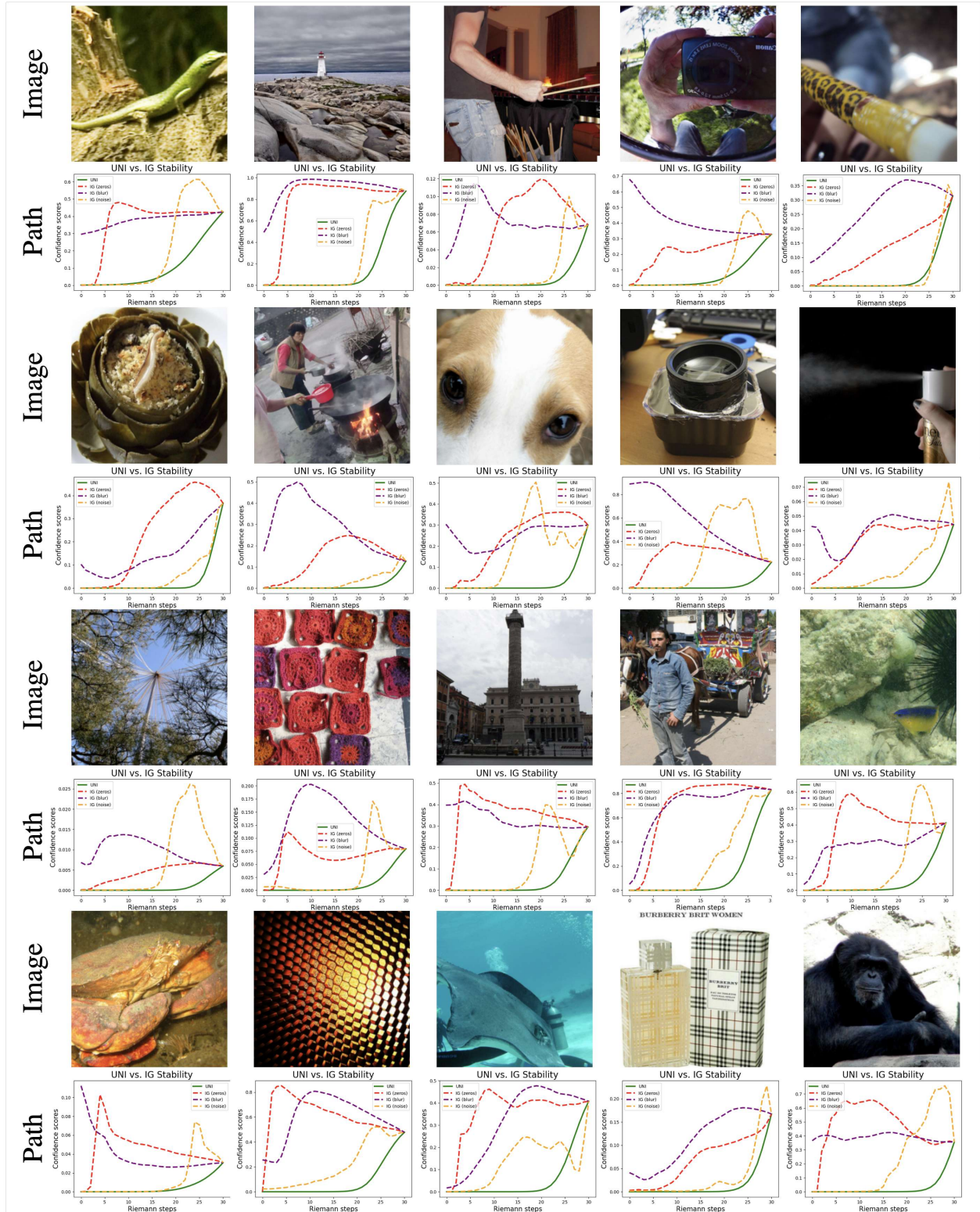
Figure 19: *Comparing paths (ConvNeXt-Tiny):* `UNI` discovers geodesic paths of monotonically increasing output confidence, preserving the completeness property required for robust attributions.

Figure 20: *Comparing paths (VGG-16-bn):* UNI discovers geodesic paths of monotonically increasing output confidence, preserving the completeness property required for robust attributions.
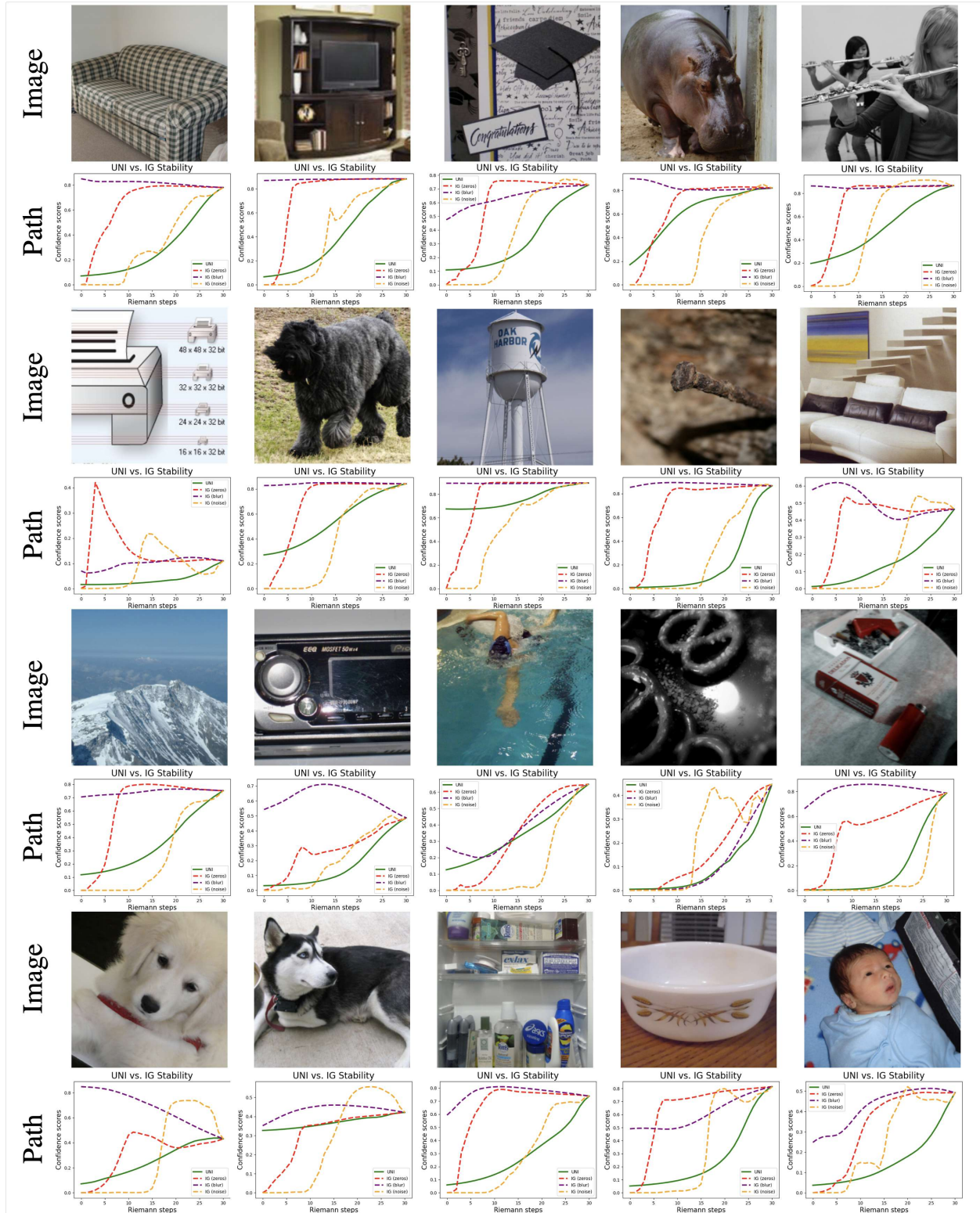
Figure 21: *Comparing paths (ViT-B_16):* `UNI` discovers geodesic paths of monotonically increasing output confidence, preserving the completeness property required for robust attributions.

Figure 22: *Comparing paths (Swin-Transformer-Tiny):* `UNI` discovers geodesic paths of monotonically increasing output confidence, preserving the completeness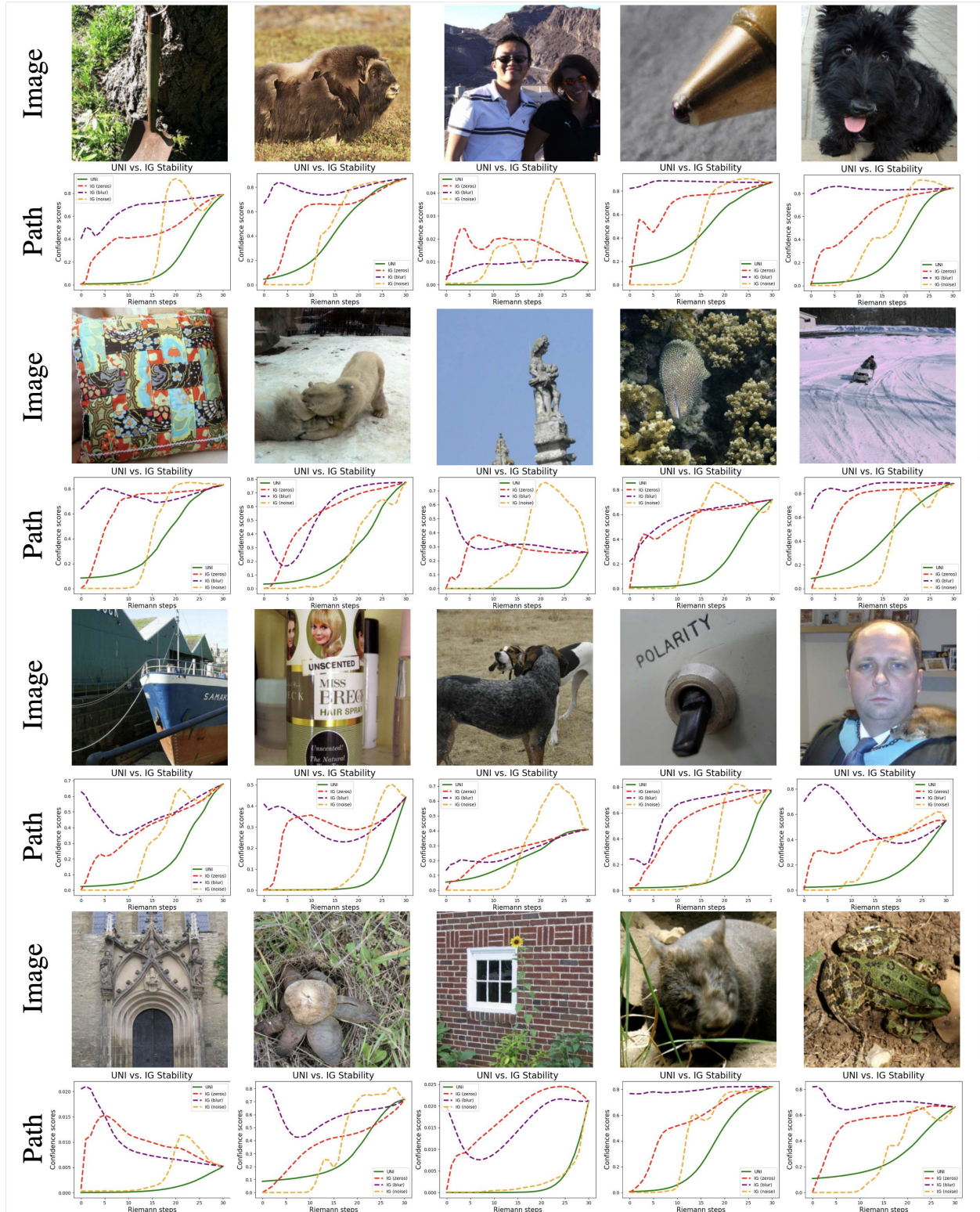 property required for robust attributions.